Understanding ACAD9 Function and the Physiologic Consequences of its Deficiency

by

Andrew Guelde Sinsheimer

BA, Oberlin College, 2008

Submitted to the Graduate Faculty of

the Department of Human Genetics

Graduate School of Public Health in partial fulfillment

of the requirements for the degree of

Doctor of Philosophy

University of Pittsburgh

2019

UNIVERSITY OF PITTSBURGH

GRADUATE SCHOOL OF PUBLIC HEALTH

This dissertation was presented

by

Andrew Guelde Sinsheimer

It was defended on

April 23, 2019

and approved by

David Finegold, MD, Professor, Human Genetics, Graduate School of Public Health, University of Pittsburgh

Eric S. Goetzman, PhD. Associate Professor, Human Genetics, Graduate School of Public Health, University of Pittsburgh

Candace Kammerer, PhD, Associate Professor, Human Genetics, Graduate School of Public Health, University of Pittsburgh

Dissertation Advisor:
Jerry Vockley, MD, PhD, Professor, Human Genetics, Graduate School of Public Health, University of Pittsburgh

Jerry Vockley, MD, PhD

Understanding ACAD9 Function and the Physiologic Consequences of its Deficiency

Andrew Guelde Sinsheimer, PhD

University of Pittsburgh, 2019

Abstract

Acyl CoA Dehydrogenase 9 (ACAD9) is a member of the family of flavoenzymes that catalyze the dehydrogenation of Acyl-CoAs to 2,3 enoyl-CoAs in mitochondrial fatty acid oxidation (FAO). Inborn errors of metabolism of nearly all family members, including ACAD9, have been described in humans, and represent significant causes of morbidity and mortality particularly in children. ACAD9 deficiency leads to a combined defect in fatty acid oxidation and oxidative phosphorylation (OXPHOS) due to a duel role in the pathways. In addition to its function in mitochondrial FAO, ACAD9 has been shown to have a second function as one of 14 factors responsible for assembly of complex I of the electron transport chain (ETC). Considerable controversy remains over the relative role of these two functions in normal physiology and the disparate clinical findings described in patients with ACAD9 deficiency.

In response to previous non-viable attempts at creating a mouse null for ACAD9 activity, several models were developed using Cre-lox to tailor knockout of the gene in specific tissues as well as allow induction of knockout in all tissues during adulthood. These models proved to have functional and biochemical phenotypes comparable to the affected tissue in humans and allowed testing of several novel therapies to assess their potential for use in humans with ACAD9 deficiency.

Tissues from these animals were also used to examine a second complex I assembly factor, Evolutionarily Conserved Signaling Intermediate in Toll pathway (ECSIT), and its interaction with ACAD9. ECSIT levels were significantly reduced in the absence of ACAD9.

These data help elucidate the physiological impact of ACAD9 deficiency, as well as provide new options for therapy of this otherwise untreatable disease. ACAD9 is the most common cause of isolated complex I deficiency in humans, underscoring the public health significance of these studies have relative to diagnosis and treatment.

Table of Contents

Preface xiv

1.0 Introduction 1

1.1 ACAD9 and its Associated Deficiency 1

1.2 Public Health Significance 4

1.3 FAO and OXPHOS 5

1.3.1 Fatty Acid Oxidation 5

1.3.2 Oxidative Phosphorylation (OXPHOS) 7

1.4 Potential Therapies for Diseases of OXPHOS 10

1.5 Cre-Lox Site-Specific Recombination 12

1.6 Hypothesis and Specific Aims 13

1.6.1 Specific Aim 1 14

1.6.1.1 Specific Aim 1a 14

1.6.1.2 Specific Aim 1b 15

1.6.1.3 Specific Aim 1c 15

1.6.2 Specific Aim 2 15

1.6.3 Specific Aim 3 16

2.0 Development of an *in vivo* Model of ACAD9 Deficiency 17

2.1 Introduction 17

2.2 Materials and Methods 18

2.3 Specific Aim 1: Results 30

2.3.1 Specific Aim 1a 30

2.3.1.1 Heart Tissue-Specific ACAD9 Deficiency Results in Viable Birth, but is Lethal Within 27 Days. 30

2.3.1.2 MRI's of Heart-Specific ACAD9 Deficient Mice Show Evidence of Cardiomyopathy Consistent with the Human Phenotype. 31

2.3.1.3 Age of Onset of Cardiomyopathy in Cardiac Tissue Specific Mutants 31

2.3.1.4 Tissue Immunohistochemistry and Protein Analysis of ACAD9 Mice 37

2.3.2 Specific Aim 1b 42

2.3.2.1 Skeletal Muscle Tissue-Specific ACAD9 Deficient Mice Show a Myopathy 42

2.3.3 Specific Aim 1c 47

2.3.3.1 Induction of a Ubiquitously Expressed Cre Gene 47

2.4 Specific Aim 1: Discussion 52

3.0 Treatment of ACAD9 Deficient Mouse Models 55

3.1 Introduction 55

3.2 Materials and Methods 56

3.3 Specific Aim 2: Results 58

3.3.1 Treatment of wild type and skeletal muscle ACAD9 deficient mice with CLBP (RTP-03?). 58

3.3.2 Treatment of wild type and ACAD9 deficient mice with JP4-039. 62

3.3.3 Treatment of skeletal muscle specific ACAD9 deficient and wild type mice with XJB-131-5. 65

3.4 Specific Aim 2: Discussion 68

4.0 Elucidating the Interaction of ECSIT in the Presence and Absence of ACAD9..... 70

4.1 Materials and Methods 71

4.2 Specific Aim 3: Results..... 74

4.2.1 An Attempt to Purify ACAD9. 74

4.2.2 Characterization of ACAD9 and ECIST Interactions in HEK 293 Cells 76

4.3 Specific Aim 3: Discussion 80

5.0 Overall Conclusions and Future Directions 81

Bibliography 86

List of Tables

Table 1. Antibodies used for Western blotting..... 26

List of Figures

Figure 1 The Predicted Three-Dimensional Structure of ACAD9 with C8 Substrate shown in the Binding 3

Figure 2 Fatty Acid Oxidation Cycle Dehydrogenation of Acyl CoA Circled 6

Figure 3 The Electron Transport Chain 8

Figure 4 The Random Diffusion Model vs. The Supercomplex Model of ETC Complex Interaction 9

Figure 5 Structures of A. JP4-039 and B. XJB-5-131 11

Figure 6 Structure of Elamipretide 13

Figure 7 Breeding Scheme for Creating Cre-lox Tissue-Specific and Inducible Mice 21

Figure 8 An 2.5% Agarose Genotyping Gel for Floxed Acad9 Mice 24

Figure 9 Hanging wire apparatus, constructed from common household hardware 28

Figure 10 MRI of p14 Mouse Hearts at Long-Axis 4-Chamber Orientation 32

Figure 11 MRI of p14 Mouse Hearts at Long-Axis 2-Chamber Orientation 33

Figure 12 MRI of p14 Mouse Hearts at Short-Axis Orientation 34

Figure 13 Comparison of Ejection Fraction Between a Single ACAD9D Mouse and WT Littermate 35

Figure 14 MRI of p3 Mouse Pups at Short-Axis Orientation 36

Figure 15 Ejection Fraction of p3 Mice Hearts 37

Figure 16 H&E Stains of Mouse Cardiac Tissue (10X) 38

Figure 17 Immunohistochemistry Stains of Cardiac Tissue-Specfic Acad9 Mouse Cardiac Tissue (40X) 39

Figure 18 Western Blots of Homogenized ACAD9D Mouse Cardiac Tissue 40

Figure 19 Blue-Native Gel Electrophoresis of Cardiac Tissue Mitochondria from ACAD9D and Wild Type Animals 41

Figure 20 Kaplan-Meier-Like Curve Measuring Fall Score of ACAD9D Skeletal Muscle-Specfic Mice 43

Figure 21 Blood L-Lactate Levels in Skeletal Muscle-Specfic ACAD9 Deficient Mice Taken Before and After a Hanging Wire Test 44

Figure 22 Immunohistochemistry Stains of Skeletal Muscle-Specfic ACAD9D Mouse Muscle Tissue with ACAD9 Antibody 45

Figure 23 Western Blot of ACAD9D Skeletal Muscle Mitochondria Using ACAD9 Antiserum 45

Figure 24 H&E (A) and Trichrome Stain (B) of Skeletal Muscle-Specfic ACAD9D Mouse Muscle Tissue 46

Figure 25 Hanging Wire Test of Induced Whole Body Induced ACAD9D Mice 48

Figure 26 Western Blot of ACAD9 in Ubiquitously Induced Acad9 Knockout Mice 49

Figure 27 Superoxide Accumulation in WBCs from Whole Body Induced ACAD9D Mice 49

Figure 28 H+E Staining (A) and Trichrome Staining (B) of Skeletal Muscle Tissue of Ubiquitously Induced Acad9 Knockout Mice 50

Figure 29 MRIs of Ubiquitously Induced ACAD9D Mice 51

Figure 30 Hanging Wire Test of Skeletal Muscle-Specific ACAD9D (ACAD9-) and Wild Type (ACAD9+) Mice Before and After (Treated) 2 Weeks of Treatment with RTP-03 59

Figure 31 Blood L-Lactate in Wild Typre Mice (A) vs. Skeletal Muscle-Specific ACAD9 Deficient Mice (B) Before and After 2 Weeks of Treatment with RTP-03 60

Figure 32 Blood Glucose Levels in Wild Type (A) and Skeletal Muscle-Specific ACAD9D Mice (B) Before and After 2 Weeks of Treatment with RTP-03 61

Figure 33 Hanging Wire Test of Skeletal Muscle-Specific ACAD9D (ACAD9-) and Wild Type (ACAD9+) Mice Before and After 2 Weeks of Treatment with JPR-039 62

Figure 34 Blood L-Lactate in Wild Type Mice (A) and Skeletal Muscle-Specific ACAD9D Mice (B) Before and After 2 Weeks of Treatment with JP$-039 63

Figure 35 Blood Glucose Levels in Wild Type Mice (A) Skeletal Muscle-Specfic ACAD9D Mice (B) Before and After 2 Weeks of Treatment with JP4-039 64

Figure 36 Hanging Wire Tests of Skeletal Muscle-Specific ACAD9D Mice Before and After (Treated) a 2 Week Treatment with XJB-5-131 65

Figure 37 L-Lactate in Wild Type (A) and Skeletal Muscle-Specific ACAD9D Mice (B) Before and After a 2 Week Treatment with XJB-5-131 66

Figure 38 Glucose Levels in Wild Type (A) and Skeletal Muscle-Specific ACAD9D Mice (B) Before and After a 2 Week Treatment with XJB-5-131 67

Figure 39 Confirmed Expression of ACAD9 in E. coli in Western Blot of Whole Cell Lysate (62 kDa) 74

Figure 40 Coomassie Stain Confirming Presence of ACAD9 in E. coli Whole-Cell Lysate After DEAE Sepharose FPLC 75

Figure 41 Western Blot for ACAD9 in Sf-21 Cells Using Whole Cell Lysate (62KDa) 76

Figure 42 Western Blot Analysis of Control HEK293 Cell Lines and a Derivative with an ACAD9 Gene Deletion 77

Figure 43 Immunohistochemistry Stains of Control and ACAD9D HEK293 Cell Lines 78

Figure 44 Western Blot Analysis of ACAD9D Mouse Cardiac Tissue 79

Preface

I have had the joy and privilege of working in the biological sciences for over a decade, and this project is the culmination of my education and ability to this point. This has been a long, and at times arduous journey. That being said, I would certainly be remiss to not acknowledge those who, without their help, these studies would not have been possible.

My mentor, Dr. Jerry Vockley, deserves the first and largest share of my gratitude. His ability to encourage and communicate such an appetite for science and research is beyond compare. I am in awe of his ability to find a twenty-fifth hour in a day for a student and still maintain a position of patience and support. He is an advisor for whom I could never be too grateful.

I would also like to thank the members of my thesis committee, Dr. Eric Goetzman, Dr. Candace Kammerer, and Dr. David Finegold. They have each been a bountiful source of support, knowledge, and drive in both the completion of this project as well as my own self-improvement as a scientist and human being.

My next round of recognitions is to my coworkers, colleagues, and friends in the Vockley lab. Anu Karunanidhi and Dr. Al-Walid Mohsen were always there for the planning and practice of every procedure and experiment and deserve so much credit for my abilities as a researcher. Dr. Lina Gonzalez, Shrabani Basu, and Dr. Yudong Wang also deserve more than notable appreciation for their invaluable tutelage. It also bears mention that Dr. Yijen Wu deserves credit for her instrumental assistance with the mouse MRI's. I also wish to extend a fond "thank you" to everyone else in the Vockley lab as well as the Goetzman lab for their friendship and

emotional support. I have never had the opportunity to work in such a friendly, and helpful environment, and I am forever thankful. Without all of them, this study would be devoid of data.

Lastly, I owe a great deal of thanks to my family and friends for their continued encouragement. From my mother, Gretchen, using a Punnett square to explain why her father and I were colorblind but she wasn't, to my lovely wife, Jessica, for letting me know when I needed to take a break (and also when I shouldn't). I am forever grateful for their love and support.

List of Abbreviations

ACAD9 – Acyl-CoA dehydrogenase family member 9

BNGE – Blue native gel electrophoresis

CBP – Cardiolipin-binding Peptide (Bendavia-like)

DMSO – Dimethyl sulfoxide

ETC – Electron transport chain

FAO – Fatty acid oxidation

FAOD – Fatty acid oxidation disorders

FBS – Fetal bovine serum

H&E – Haemotoxylin and Eosin

HWT – Hanging Wire Test

IF – Immunofluorescence

IHC – Immunohistochemistry

PBS – Phosphate buffered saline

PBST – Phosphate buffered saline with Tween 20

ROS – Reactive oxygen species

SDS-PAGE – Sodium dodecyl sulfate polyacrylamide gel electrophoresis

WB – Western blot

1.0 Introduction

1.1 ACAD9 and its Associated Deficiency

Acyl-CoA dehydrogenase 9 (ACAD9) is a member of acyl-CoA dehydrogenase (ACAD) gene family, which encodes enzymes involved in the catalysis of α, β dehydrogenation of acyl-CoA esters during fatty acid β-oxidation and branched chain amino acid catabolism in mitochondria.

ACAD9 exhibits maximum activity with unsaturated long-chain fatty acids such as palmitoyl-CoA (C16), similar to very long chain acyl-CoA dehydrogenase (VLCAD)[1]. Despite this substrate overlap, these two proteins have separate and distinct physiologic functions and deficiency of one is not rescued by the presence of the other[7]. Treatment for β-oxidation deficiencies is a low fat/high glucose diet to reduce the build-up of intermediates within the fatty acid cycle, as well as avoiding fasting and intense exercise[9].

ACAD9 is unique among the ACADs in that it has a secondary function (often denoted as "moonlighting") in the assembly of complex I of the mitochondrial electron transfer chain (ETC)[3]. Complex I (NADH ubiquinone oxidoreductase) is the largest complex of the ETC, located primarily in the inner mitochondrial membrane, but with an $NADH^+$ binding domain that extends into the mitochondrial matrix[10]. The latter domain accepts reducing equivalents from a variety of mitochondrial dehydrogenases as the first step in oxidative phosphorylation (OXPHOS), which generates a proton gradient across the inner membrane that is ultimately used by complex V to synthesize ATP. Complex I is composed of 45 structural subunits, requiring at least 14 additional proteins for proper assembly, including ECSIT and NDUFAF1, both binding

partners with ACAD9 in the assembly process[11,12]. Symptoms of ACAD9 deficiency are variable and include cardiomyopathy, liver dysfunction, episodic metabolic decompensation, and hypotonia[13]. Deficits of both functions of ACAD9 contribute to the phenotype of an ACAD9 deficient patient, particularly in tissues where ACAD9 is highly expressed including the liver, heart, and brain. Specifically, mutations in ACAD9 protein that affect both the chaperonin and enzymatic functions lead to more severe clinical symptoms than those that affect only the complex I assembly function[3].

The ACAD9 gene is located on chromosome 3q21.3 and is comprised of 18 exons encoding a precursor protein of 621 amino acids with a molecular mass of 68 kDa[14]. The precursor protein is imported into mitochondria and processed to its mature form through the action of two mitochondrial peptidases that cleave a 37 amino acid sequence from the N-terminus end before the mature protein assembles as a homodimer associated with the inner mitochondrial membrane[15]. The existing three-dimensional model of the structure of ACAD9 uses VLCAD's known structure as a template (Figure 1). ACAD9 shares the greatest sequence homology with VLCAD, also a homodimer, while the other ACADs are tetramers. However, the two proteins share only 47% homology[16].

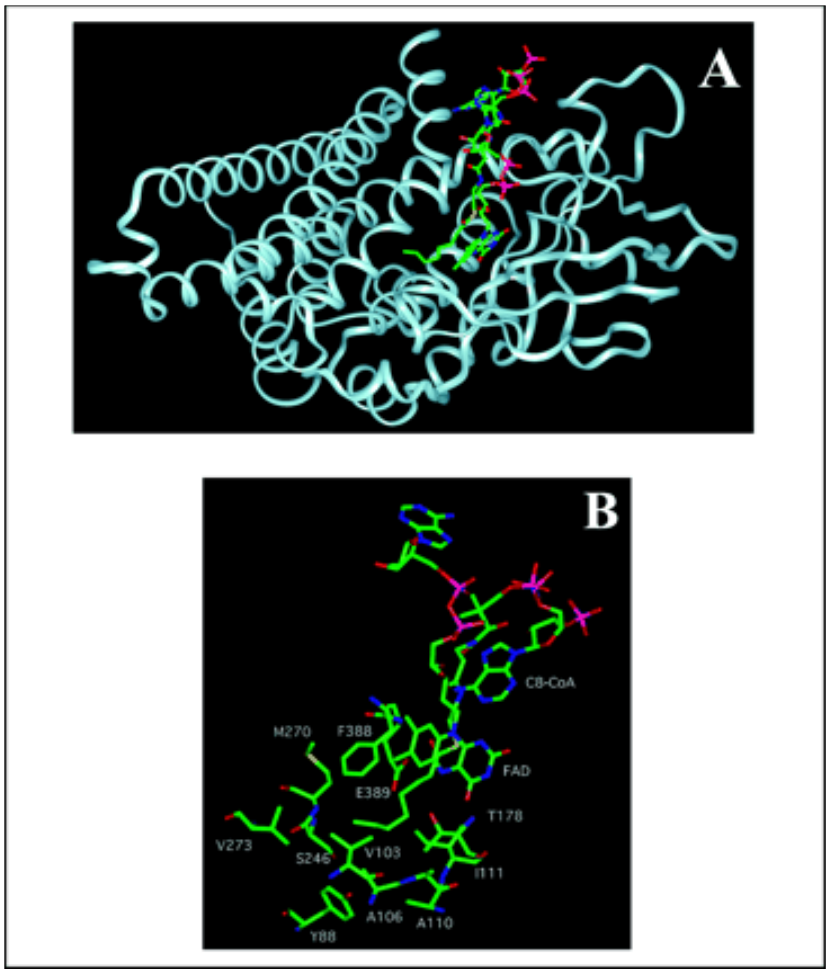

Figure 1 The Predicted Three-Dimensional Structure of ACAD9 with C8 Substrate shown in the Binding

A. Ribbon representation of one monomer of the dimeric structure with FAD and substrate bound in catalytic site. B. Detailed view of substrate and FAD interaction with key amino acid residues. For FAD and substrate, carbon atoms are shown in green, nitrogen atoms in red, and oxygen atoms in blue.

1.2 Public Health Significance

Inborn errors of metabolism are individually rare but in total are present in ~0.5% of all babies born in the U.S. though symptoms may not present until adulthood[17]. Deficiencies of most of the ACADs have been described including short chain- (SCAD), medium chain- (MCAD), very long-acyl-CoA dehydrogenases (VLCAD), and ACAD9[7]. These disorders lead to fasting or stress induced hypoglycemia due to the reduced energy generating capacity of cells, and to a potentially toxic accumulation of acyl-CoAs and acylcarnitines. Most individuals with these disorders are identified through expanded newborn screening. Current projections estimate the worldwide incidence of ACAD9 deficiency to be nearly 700 cases a year[38]. Deficiency of ACAD9 presents predominantly as a disorder of OXPHOS and cannot be identified through newborn screening. Thus patients are only identified through clinical symptoms, often with life threatening cardiomyopathy within the first five years of life, and others living longer only to succumb to a Reye-like episode and cerebellar stroke with metabolic stress[18]. In one study, 8/20 patients presenting with complex I deficiency and cardiomyopathy had ACAD9 deficiency detected through whole-exome sequencing [12].

Many patients with later onset ACAD9 related complex I deficiency respond to riboflavin; however, others do not, especially neonates, and may progress to fatal heart failure[38]. Heart transplant was successful as treatment for complex I deficiency-related cardiomyopathy, but did not alleviate other symptoms[12]. Thus additional understanding of the pathophysiology of ACAD9 and development of better therapies will represent a significant public health benefit towards the treatment of ACAD9 deficient patients as well as other sufferers of inborn errors of metabolism.

1.3 FAO and OXPHOS

1.3.1 Fatty Acid Oxidation

Fatty acids are the most energetic per gram of all macromolecular nutrients, with one molecule of palmitoyl-CoA (C16) yielding 129 molecules of ATP[1]. Fatty acids can also function as chemical messengers within the cell. During times of fasting or physiologic stress, fatty acids are liberated from tissue stores as free fatty acids, transported into cells, activated to a coenzyme-A intermediate, and transported into the mitochondrial matrix, where it then undergoes a four-step process known as FAO or β-oxidation (3) (Figure 2.):

1. Dehydrogenation (catalyzed by a member of the family of ACADs) in which hydrogen atoms are removed from carbons 2 and 3 of the fatty-acid chain and added to two molecules of FAD forming a trans-enoyl-CoA and $FADH_2$, with a double bond between C-2 and C-3. (Circled in Figure 2.)
2. Hydration of the C-2 and C-3 bond of the trans enoyl-CoA to form L-3-hydroxyacyl-CoA.
3. Dehydrogenation of L-3-hydroyacyl-CoA by NAD to form a 3-ketoacyl-CoA and NADH.
4. Thiolysis of the 3-ketoacyl-CoA, generating an acetyl-CoA group and leaving an acyl-CoA that is two carbons shorter than the original substrate, ready to enter the cycle again, as well as NADH and $FADH_2$ which are substrates for oxidative phosphorylation.

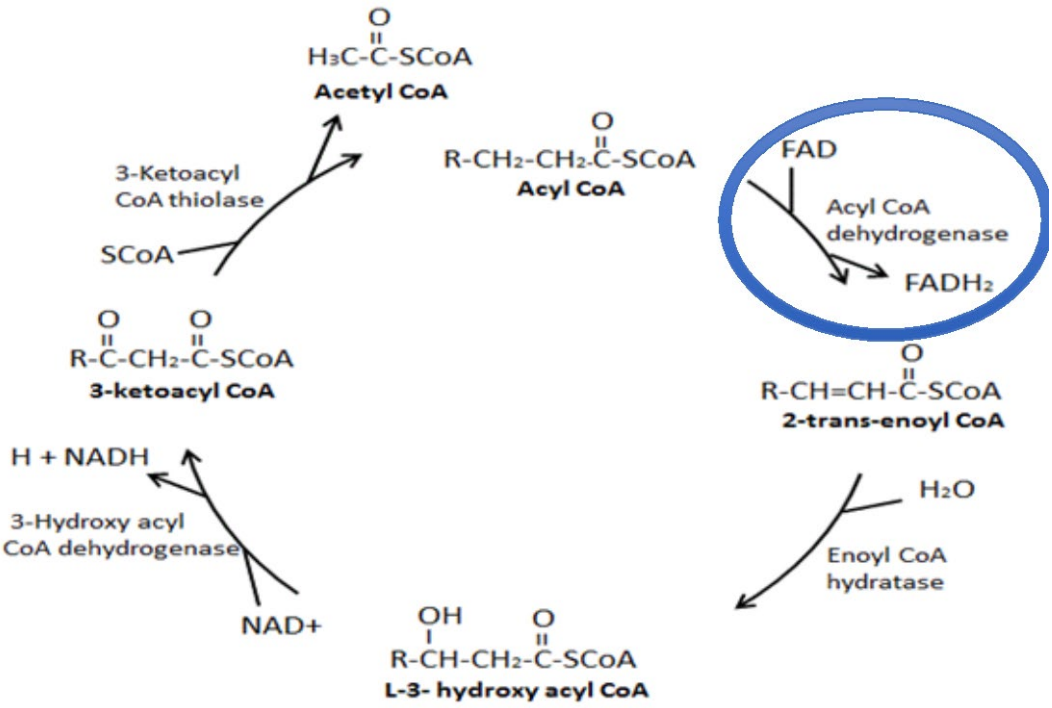

Figure 2 Fatty Acid Oxidation Cycle Dehydrogenation of Acyl CoA Circled

A representation of the Fatty Acid Oxidation Cycle, highlighting the dehydrogenation of Acyl CoA enzymatically forwarded by the ACAD family (including ACAD9) in which two hydrogen atoms are transferred from Acyl CoA to the coenzyme FAD. This results in 2-trans-enoyl CoA which in turn continues through the remainder of the FAO cycle. Image comes from the AOCS Lipid Library https://lipidlibrary.aocs.org/chemistry/physics/animal-lipids/fatty-acid-beta-oxidation. Authors: Natasha Fillmore, Osama Abo Alrob and Gary D. Lopaschuk.

In humans, some tissues are more dependent on FAO than others. For instance, the heart depends on fatty acid metabolism for ~75% of its energy[4]. Also, during exercise or fasting, when glucose levels are low, skeletal muscle will consume fatty acids for energy, and the liver will convert fatty acids into ketone bodies to be used by organs such as the brain that depend heavily on glucose, but lack the capabilities to process long-chain fatty acids[5]. At least 25 different enzymes and carriers are known to be involved in β-oxidation, and deficiencies of most of them have been identified as inborn errors of metabolism[6]. As in many cellular pathways, lacking the

necessary enzyme to catalyze a reaction has two effects. The first is a deficit of the product of the pathway (energy in the case of FAO disorders), leading to a large number of symptoms related to specific tissues and including hypoglycemia, muscle weakness, and heart failure[7]. The second is a build-up of intermediary metabolism molecules that can lead to cardiac arrhythmias, central nervous dysfunction, and sudden unexpected death.

1.3.2 Oxidative Phosphorylation (OXPHOS)

OXPHOS is the cellular process by which ADP is converted into ATP through energetically favorable electron transfer from NADH and $FADH_2$ to molecular oxygen[8]. The protein complexes that act as carriers that facilitate the transfer of the electrons from the high-energy to low-energy state form the electron transport chain (ETC) (Figure 3). Complex I (NADH-ubiquinone oxidoreductase) begins the process of OXPHOS by catalyzing the oxidation of NADH (acquired from LCHAD of FAO and other mitochondrial dehydrogenases) to NAD^+. This protein complex consists of 46 different subunits including distinct iron-sulfur clusters which aid in the transfer of electrons from NADH to ubiquinone. This transfer of electrons is coupled with the movement of 4 protons across the inner mitochondrial membrane, approximately three of which are required for the generation of 1 equivalent of ATP[23]. The ETC is localized to the cristae of the inner mitochondrial membrane where it is associated with the proteins of FAO, forming a large macromolecular energy protein complex[36].

It should be noted that the major individual complexes that act as proton pumps to establish a charge across the inner mitochondrial membrane (complexes I, III, and IV) were originally thought to be located independently within the inner mitochondrial membrane and interact using a random diffusion model. In other words, the product of one complex would react

with the following enzyme in the ETC by random association[31]. More recent studies have identified that complexes I, III, and IV associate in the form of supercomplexes that increase their interactive efficiency[32].

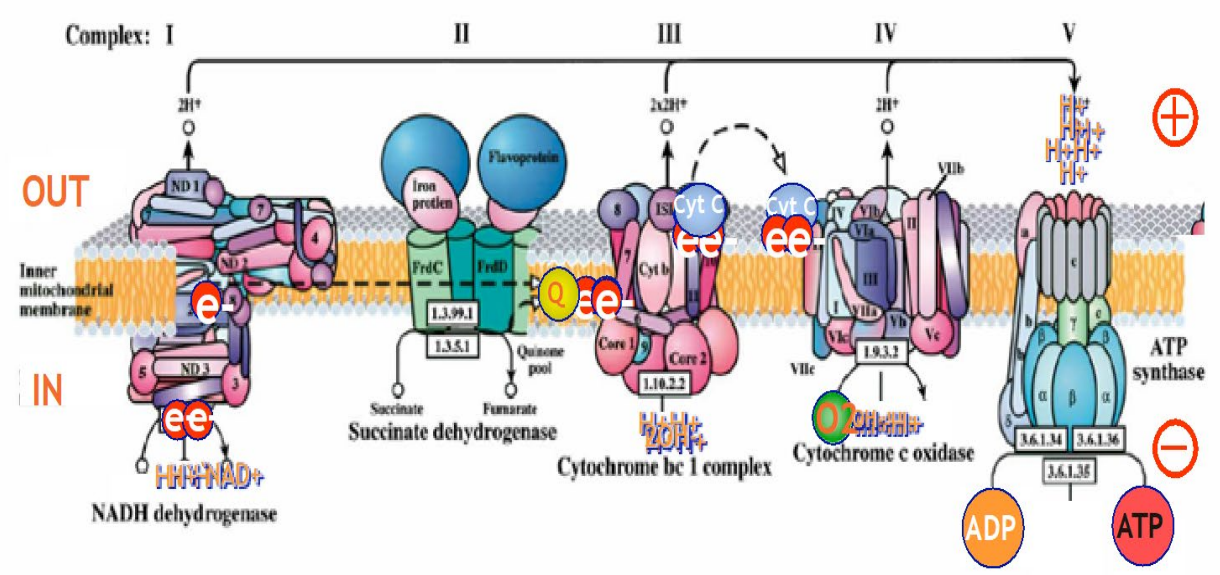

Figure 3 The Electron Transport Chain

A diagram demonstrating the flow of electrons through the electron transport chain (symbolized by the smaller arrows) and the establishment of a proton gradient across the inner mitochondrial membrane generating ATP and water. Complex I is of particular note for its role in beginning the process by oxidizing NADH and transferring the electrons to ubiquinone.

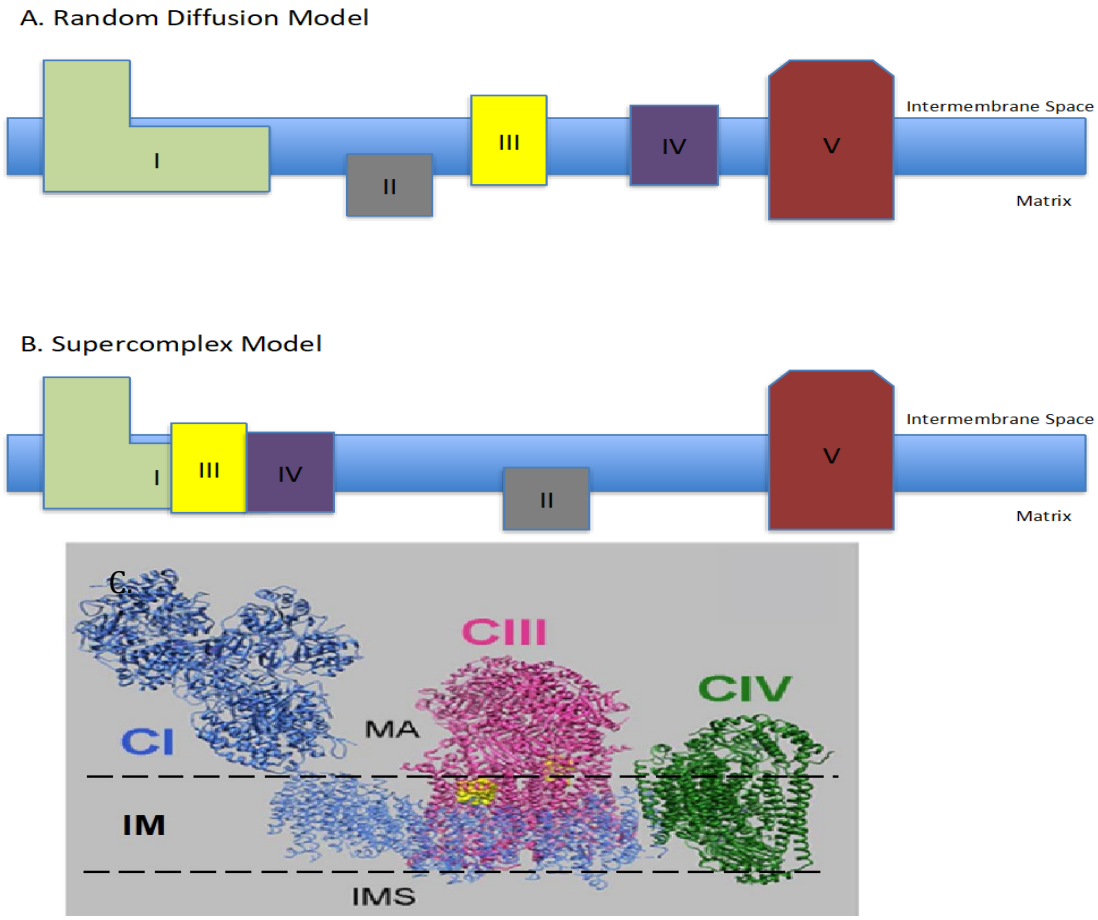

Figure 4 The Random Diffusion Model vs. The Supercomplex Model of ETC Complex Interaction

A. Older models of OXPHOS complex interactions envisioned reliance on random interaction of products and substrates colliding with one another within the three dimensional space of the inner mitochondrial membrane. B. The current model, which shows the interaction between complexes I, III, and IV, leading to increased efficiency. C. A detailed protein model of the supercomplex with dashed lines indicating the inner mitochondrial membrane.

1.4 Potential Therapies for Diseases of OXPHOS

Diseases of OXPHOS are pleiotropic and induce several cellular mechanisms of pathophysiology. One mechanism of damage is related to oxidative stress caused by an increase in reactive oxygen species caused by physical incompetence of the ETC. Therefore, antioxidants have long been hypothesized to be candidates for treatment of OXPHOS disorders, and have shown some efficacy *in vitro*[37]. Unfortunately, most of these compounds have shown little effect in clinical studies on patients. The Vockley lab has been investigating several novel compounds designed to treat oxidative stress that have proven to be more potent than previous antioxidants *in vitro* and appear to be good candidates for treating OXPHOS disorders[27].

The first two compounds are both gramicidin-S-nitroxides, JP4-039,and XJB-5-131, designed and synthesized by Dr. Peter Wipf of the University of Pittsburgh, initially to mitigate oxidative stress due to mitochondrial dysfunction in Huntington disease and radiation induced tissue damage [28,29]. Their mechanism of action relies on a highly-reactive 4-amino-tempo site linked to moieties that allow them to localize to mitochondria resulting in higher levels of antioxidant activity than other currently available molecules (Figure 5). The third compound also has a high affinity for targeting mitochondria, binding directly to the inner mitochondrial membrane specific lipid cardiolipin, a molecule critical for maintaining the inner mitochondrial membrane shape and mitochondrial stability. This cardiolipin binding peptide (designated RTP-03) is a structural analogue of elamipretide (Figure 6; also known as bendavia or SS-31), a medication currently in clinical trials for the treatment of mitochondrial respiratory chain deficiencies[39]. An aromatic tetrapeptide, elamipritide is proposed to stabilize abnormal cardiolipin, restore the inner mitochondrial membrane integrity, and increase OXPHOS[30]. The behavior of this particular peptide would suggest that if there is sufficient complex I, and

therefore supercomplex activity, that OXPHOS activity could be rescued sufficiently to ameliorate the loss of function caused by ACAD9D.

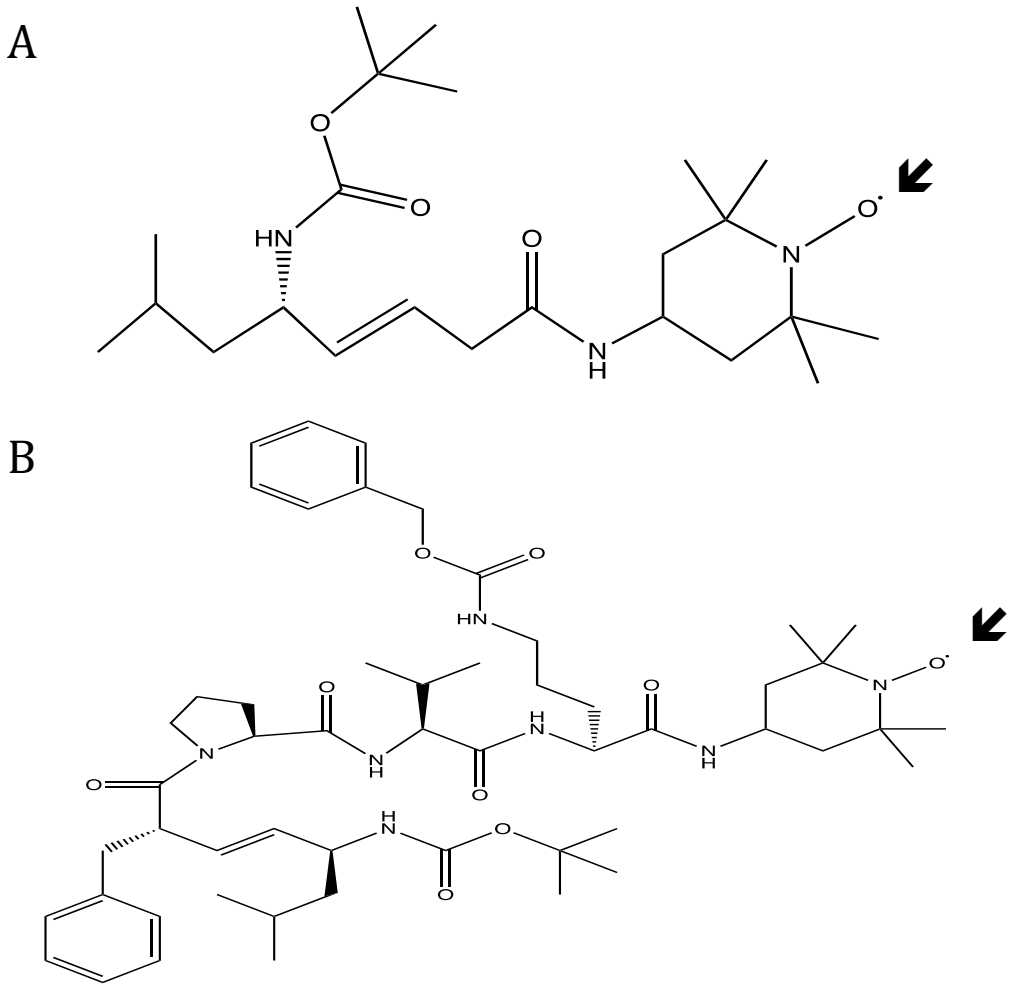

Figure 5 Structures of A. JP4-039 and B. XJB-5-131

See text for full description. Both compounds have a characteristic 4-amino-Tempo (shown with an arrow) responsible for high reactivity with free radicals within the mitochondria.[27]

1.5 Cre-Lox Site-Specific Recombination

While it is often useful to genetically inactivate (knock-out) a specific gene to observe disruption of its function *in vivo*, this can prove limiting if the gene in question is necessary for the viability of the organism. In such cases, other methods are required to characterize the function of a given gene. Cre-Lox recombination is one such method that enables tissue-specific, and even temporal-specific, knockout of a particular gene. This allows for the ability to observe a phenotype in an animal such as a mouse where the knockout of the gene would otherwise be non-viable.

Cre, or the **C**auses **Re**combinase protein, is derived from the P1 bacteriophage and targets specific sites in DNA known as lox*p* (Locus of X over P1). Lox*p* sites are small palindromic sites which can be inserted on both ends of a particular exon or gene, which is then referred to as being "floxed." Cre then targets the lox*p* sites and excises the floxed region. In animal models, organisms can be bred to be homozygous for a floxed gene and then bred with an individual that has the Cre gene linked to a promoter that is tissue specific. Once the tissue of interest begins producing Cre, the floxed gene will be excised, but only in the specific tissue rather than ubiquitously. Similarly, tissue-specific, or even whole-body genetic deletions can be induced after birth in animal models by linking the *Cre* gene to the promoter of a ubiquitously expressed gene, but also attached to a domain of an estrogen receptor. This receptor domain prevents Cre from crossing the nuclear membrane, and thus prevents recombination. When exposed to tamoxifen, the estrogen receptor domain will bind to the drug, allow for Cre to translocate to the nucleus, and the excision of the gene can take place at a later stage in the animal's development. With this tool, a mutation can be created in an adult animal model that otherwise would have been lethal at a younger age.

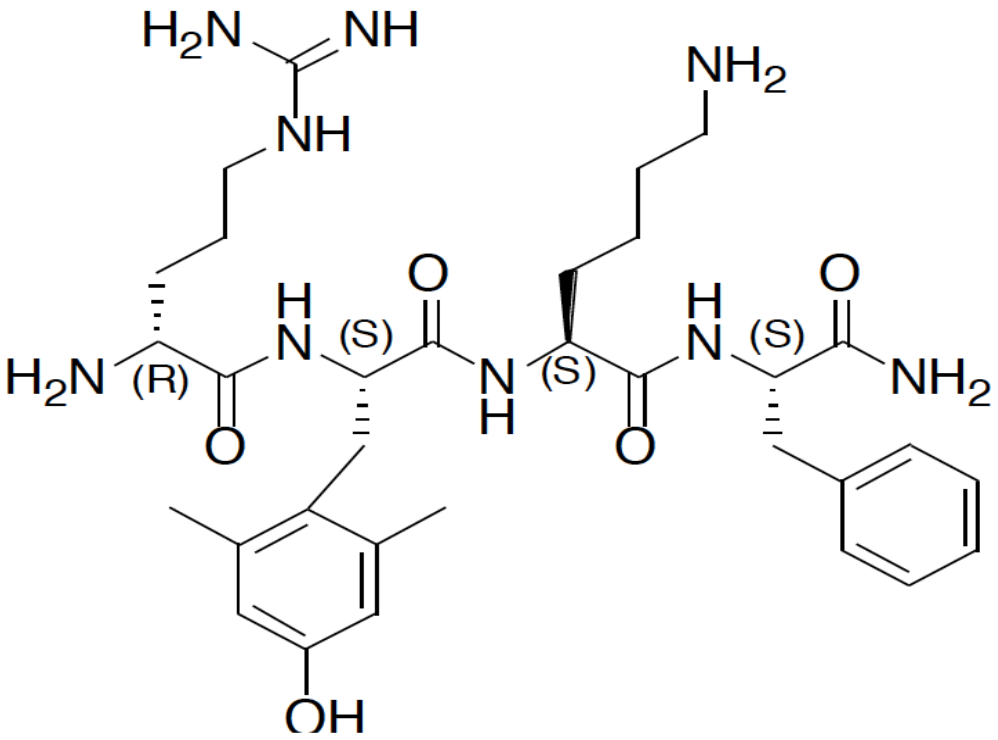

Figure 6 Structure of Elamipretide

See full description in text. Elamipretide is a structural analogue of the cardiolipin binding peptide investigated in this thesis, and shares the same properties, resulting in stabilization of the inner mitochondrial membrane.

1.6 Hypothesis and Specific Aims

The overall goal of this project was to better characterize the physiologic function and biochemical characteristics of ACAD9, and to assess the consequences of its deficiency. ACAD9 is a member of the acyl-CoA dehydrogenase (ACAD) gene family whose members are involved in mitochondrial fatty acid oxidation (FAO) and branched chain amino acid catabolism[1]. Inborn errors of metabolism of all family members, including ACAD9, have been described in humans, and represent significant causes of morbidity and mortality especially in children. ACAD9

deficiency leads to a combined defect in fatty acid oxidation and oxidative phosphorylation (OXPHOS) due to differing roles in each pathway. In addition to functioning enzymatically in the first mitochondrial matrix step of FAO, ACAD9 has been shown to have a moonlighting function as an assembly factor for complex I of the electron transport chain (ETC)[2]. Considerable controversy remains over the relative role of these two functions in normal physiology and the disparate clinical findings described in patients with ACAD9 deficiency. My project has the following three aims:

1.6.1 Specific Aim 1

To create an animal model of ACAD9 deficiency that appropriately mirrors the human phenotype. Preliminary data suggest that complete ACAD9 deficiency is lethal in a mouse. I hypothesize that tissue-specific and/or time limited deficiency will lead to viable animals with a subset of human symptoms. These models will provide an opportunity to study the pathophysiology of ACAD9 deficiency as well as explore therapeutic options. I have separated each of these models into their own sub-aims.

1.6.1.1 Specific Aim 1a

To create a mouse model that demonstrates ACAD9 deficiency in cardiac tissue. I hypothesized that the mouse would develop cardiomyopathy, consistent with human patients with ACAD9 deficiency.

1.6.1.2 Specific Aim 1b

To create a mouse model that demonstrates ACAD9 deficiency in the skeletal muscle. I hypothesized the mouse would have similar myopathic phenotype to human patients.

1.6.1.3 Specific Aim 1c

To create a mouse model in which whole body ACAD9 deficiency can be induced after birth. I hypothesized that after induction, the mice would show significant systemic symptoms caused by global OXPHOS deficiency.

1.6.2 Specific Aim 2

To use the various ACAD9 deficient mouse models to test therapeutic compounds as treatment for ACAD9 deficiency. The first compound is a cardiolipin binding peptide (RTP-03) that stabilizes inner mitochondrial membranes, improving ETC activity and reducing superoxide production. I hypothesized that since ACAD9 deficient mice should have little to no complex I and ETC super-complexes, that the peptide would have minimal impact on the phenotype of the mice. The second and third treatments were with JP4-039 and XJB-5-131, mitochondrial targeted antioxidants designed by our collaborator Dr. Peter Wipf of the Department of Chemistry at the University of Pittsburgh. I predicted that this treatment would reduce intramitochondrial ROS in ACAD9 deficient mitochondria and improve ETC function, resulting in clinical improvement in ACAD9 deficient mice.

1.6.3 Specific Aim 3

To examine the effect of ACAD9 deficiency on ECSIT, another complex I assembly factor known to interact with ACAD9. I hypothesized that ECSIT protein levels will be reduced or absent in ACAD9 tissues consistent with previous studies in ACAD9 deficient tissue culture cells.

2.0 Development of an *in vivo* Model of ACAD9 Deficiency

2.1 Introduction

An *in vivo* model of a disease phenotype is invaluable for the study of rare congenital diseases. However, in some cases completely deficient animal models are nonviable. Knock out of the ACAD9 gene by the Vockley lab resulted in litters with no affected pups suggesting embryonic lethality. To address this issue, Cre-lox technology can be utilized to delete ACAD9 in a tissue specific fashion that results in a tissue limited phenotypes associated, but is still viable. In addition to tissue-specific knockout variants, it is also possible to induce the knockout of a gene later in life leading to a temporal limited phenotype. This allows for a ubiquitous deficiency of the gene, but guarantees that the mouse survives birth, only exhibiting symptoms in a time specific fashion. The goal of my first aim was to develop three separate *in vivo* mouse models of ACAD9 deficiency. Two of these were tissue specific, restricted to cardiac and skeletal muscle, the primary tissues involved in humans. The third model was a ubiquitous ACAD9 deficiency induced in adulthood.

2.2 Materials and Methods

Materials:

All items were purchased from Millipore Sigma, St. Louis, MO unless otherwise noted.

Animal Materials:

All mice stains were provided by the Jackson Laboratories (Bar Harbor, ME). The following Cre positive strains were purchased with the given descriptions from Jackson Laboratories:

FVB-Tg(Myh6-cre)2182Mds/J. The cardiac-specific alpha myosin-heavy chain (*Myh6*, myosin, heavy polypeptide 6, cardiac muscle, alpha) promoter drives expression of cre in this transgenic strain. The promoter induces greater than 90% recombination in cardiac muscle cells. The transgenic construct contained the *Myh7* 3' untranslated region, the *Myhca* promoter, *Myhca* noncoding exons 1 and 2, and the exon 3 splice acceptor site 180 bp upstream and driving the expression of the cre recombinase sequence. The *Myhca* promoter drives expression in cardiac tissue.

FVB.Cg-Tg(ACTA1-cre)79Jme/J. These transgenic mice have the cre recombinase gene driven by the human alpha-skeletal actin (*HSA* or *ACTA1*) promoter. When bred with mice containing a lox*p*-flanked sequence of interest, Cre-mediated recombination will result in striated muscle-specific deletion of the flanked genome. This transgene expresses Cre recombinase under the control of a human alpha-skeletal actin promoter, active in striated muscle, heart, and skeletal muscle.

Tg(UBC-cre/ERT2)1Ejb. These transgenic mice express a *Cre-ERT2* fusion gene under the control of the human ubiquitin C (UBC) promoter. The transgene integrated into chromosome 2 causing an 5 bp deletion in *Ndor1* (NADPH dependent diflavin oxidoreductase 1). Mice hemizygous for this *Cre-ERT2* transgene are viable and fertile. Mice from this founder line have strong tamoxifen-inducible *cre* activity in all reported tissue types. The *Cre-ERT2* fusion protein consists of Cre recombinase fused to a triple mutant form of the human estrogen receptor; which does not bind its natural ligand (17β-estradiol) at physiological concentrations but will bind the synthetic estrogen receptor ligands 4-hydroxytamoxifen (OHT) and, with lesser sensitivity, ICI 182780. Restricted to the cytoplasm, *Cre-E*RT2 can only gain access to the nuclear compartment after exposure to OHT. To counteract the mixed estrogen agonist effects of tamoxifen injections, which can result in late fetal abortions in pregnant mice, progesterone may be co-administered. When these *Cre-ERT2* mice are bred with mice containing a *loxP*-flanked sequence of interest, tamoxifen-inducible, Cre-mediated recombination will result in deletion of the flanked sequences in widespread cells/tissues.

Primers: All primers were ordered from ThermoFisher Scientific (Waltham, MA). Sequences are listed below:

Acad9-Forward: TCTAGCTCTTCAGCAAGTGCTTCCC

Acad9-Reverse: AGTGTTCATTTCCTGCTGTGTGAGC.

Reverse complement: GCTCACACAGCAGGAAATGAACACT)

Primers to detect FVB-Tg(Myh6-cre)2182Mds/J (Cardiac Specific Cre):

9543 (Transgene Forward): ATGACAGACAGATCCCTCCTATCTCC

9544 (Transgene Reverse): CTCATCACTCGTTGCATCATCGAC

PCR product: ~300bp

Primers to detect FVB.Cg-Tg (ACTA1-cre) 79Jme/J (Skeletal Muscle Specific Cre):

oIMR1084 (Transgene Forward): GCGGTCTGGCAGTAAAAACTATC

oIMR1085 (Transgene Reverse): GTGAAACAGCATTGCTGTCACTT

PCR product: ~100 bp

Primers to detect Tg(UBC-cre/ERT2) 1Ejb (Inducible Whole Body Cre):

oIMR1084 (Transgene Forward): GCGGTCTGGCAGTAAAAACTATC

oIMR1085 (Transgene Reverse): GTGAAACAGCATTGCTGTCACTT

Mouse Breeding:

Transgenic insertion of the *Loxp* sites to book-end exon 3 of the ACAD9 gene created a floxed gene that when targeted for recombination deleted the region of the gene and inactivate the gene. After successfully creating mice with the floxed gene, I was able to breed the heterozygotes for the floxed genes with each other to create homozygous floxed mice. ACAD9 floxed mice were then bred with one of three different partners: a *Cre* gene driven from a heart promoter, a skeletal muscle promoter, or a ubiquitous promoter activated through exposure to tamoxifen. These mice were bred with homozygous *Cre* mice, and 25% of the offspring were expected to be homozygous for the floxed allele and have one copy of the *Cre* allele (Figure 7).

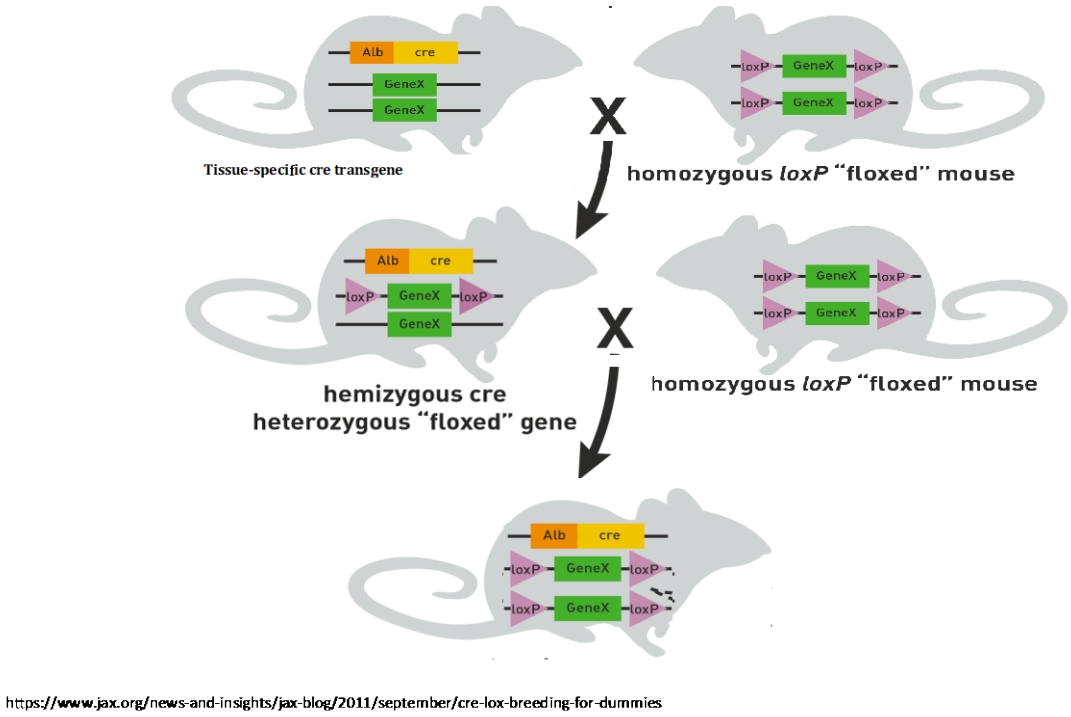

Figure 7 Breeding Scheme for Creating Cre-lox Tissue-Specific and Inducible Mice

See test for a description of each strain and cross. Image is printed with permission from © Jackson Laboratories https://www.jax.org/news-and-insights/jax-blog/2011/september/cre-lox-breeding-for-dummies

Mice were housed and bred according to AALAC guidelines with the following specific considerations. Tails tips were snipped at day 14 for genomic DNA extraction and genotyping as described below. Litters were weaned and placed in separate cages according to sex, on day 21 to reduce the risk of two litters being present in the cage at once. Males were maintained no more than 4 to a single cage, and only littermates that had never been separated were kept together to avoid fighting. Females were maintained no more than 5 to a single cage. All mice of the same sex were identified by coat color (black, grey, or white) and by ear punch (none, left, right, both).

Extraction of Genomic DNA for the Purpose of Genotyping:

At the age of 2 weeks, the tip of the tail (approximately 3 mm) was removed from the mouse and placed in 700 µL of fresh genomic DNA extraction buffer (7.8 mL ddH_20; 15 µL Proteinase K; 1 mL 1M Tris buffer, pH 8.0; 500 µL 20% SDS; 500 µL 0.5M EDTA, pH 8.0; 200 µL 5M NaCl). The buffer and tail were left on a lab sample rotator overnight at 55 °C. Phenol/chloroform/isoamyl alcohol (700 µL) was added to the now dissolved tail sample. The sample was shaken vigorously for one minute, left to rotate for 10 minutes at room temperature, then centrifuged in a microfuge for 10 minutes at 16,128 x g The top aqueous layer was moved to another Eppendorf tube and 700 µL of pure chloroform were added to the sample, shaken vigorously for a minute at room temperature, left to rotate for 10 minutes, and centrifuged for 10 minutes at 16,128 x g. The aqueous phase was again saved, 700 µL of isopropanol were added to the sample, and the tube was gently inverted ten times until the DNA began to precipitate. The sample was centrifuged in a microfuge for 3 minutes at 2,268 x g and the isopropanol was decanted. One milliliter of 70% ethanol was added to wash the pellet and centrifuged for 3 minutes at 2,268 x g and the ethanol was decanted. One milliliter of 100% ethanol was added to

wash the pellet for a second time, and the sample was centrifuged a final time for 3 minutes at 2,268 x g. Finally, the 100% ethanol was decanted, and the pellet was left to dry at room temperature for 15-30 minutes. After the pellet was completely dry, 80 µL of doubly distilled water (ddH_20) were added to resuspend the pellet, and the sample was incubated at 37 °C overnight. The samples were then measured for DNA concentration with a nanodrop instrument (Thermofisher, Waltham, MA).

Genotyping Genomic DNA of Mouse models:

Two microliters containing 100-300 ng of the DNA were added to fresh PCR reaction buffer (Thermofisher, Waltham, MA). The mixture was then was placed in a thermocycler (S1000, Bio-Rad, Hercules, CA) and run with the following program:

1. 94 °C for 5 minutes
2. 94 °C for 1 minute
3. 52 °C for 1 minute
4. 72 °C for 1 minute
5. Repeat steps 2-4 35 times
6. 72 °C for 10 minutes
7. 4 °C on hold

Following PCR, samples were mixed with 2.5 µL of BlueJuice™ 10x gel loading dye (Thermo Fisher, Waltham, MA) and separated by electrophoresis on a 2.5% agarose gel at 90 mV for 30-60 minutes. The gel was visualized with UV light and photographed. An example of a genotyping gel is shown demonstrating examples of the floxed and wildtype bands of ACAD9 (Figure 8).

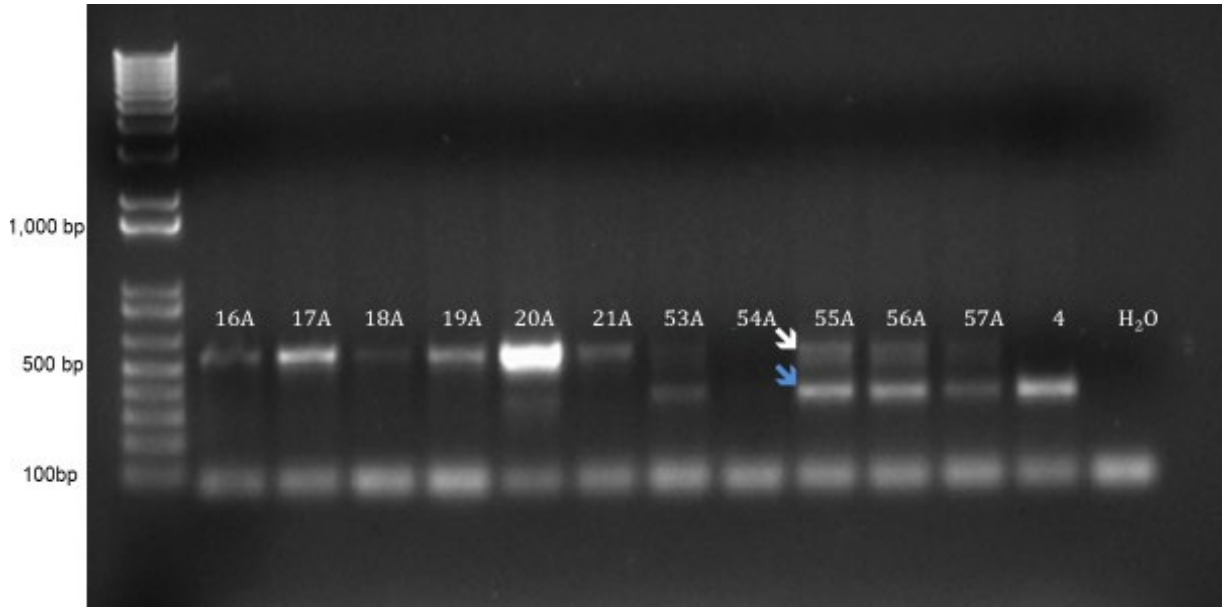

Figure 8 An 2.5% Agarose Genotyping Gel for Floxed Acad9 Mice

The floxed gene yields a band that is larger than the wildtype allele on agarose gel electrophoresis. In this example, mice 16A through 21A are homozygous for the floxed allele. 53A,55A, 56A, and 57A are heterozygotes as indicated by the presence of an expected ~538 bp band (white arrow), and mouse 4 (control) is homozygous for the wildtype allele of *Acad9* as indicated by a ~349 bp band (blue arrow). 54A was inconclusive. Water was used as a negative control. The 100 bp ladder starts with 100 bp as the lowest band.

Extracting mouse tissue for processing and protein analysis:

Mice were euthanized by CO_2 asphyxia followed by cervical dislocation. Mouse heart, liver, and skeletal muscle were excised, and each tissue was washed in ice-cold PBS until clear of blood. Tissues were cut into two (ratio of approximately 25:75), and the smaller piece of

tissue was treated with 4% paraformaldehyde, which was then submitted for histology analysis by the UPMC Children's Hospital Histology Core, including immunohistochemistry, and haemotoxylin and eosin staining (H&E) and trichrome staining. The larger piece of tissue was placed in a cryofreeze-safe tube and immediately submerged in liquid nitrogen to flash freeze. The sample was stored at -80 °C.

Isolating Mitochondria from Whole Tissue:

Mouse tissue was placed in ice-cold homogenization buffer (HB; 3mM KH_2PO_4, 47mM K_2HPO_4, 1mM EDTA, 215 mM sucrose, 10% glycerol) containing a protease inhibitor cocktail tablet (MilliporSigma) (1 tablet per 50 mL of HB). The tissue was sheared using an electric homogenizer (Handishear, Virtis, Gardiner, NY) for 10-second intervals on ice until no large pieces of tissue were observed. The sample was then centrifuged at 512 x g for 10 minutes. The supernatant was transferred to another vial and more ice-cold HB buffer was added to resuspend the pellet, and the process was repeated. The final supernatant was centrifuged at 20,000 x g rpm for 20 min, and the supernatant was discarded. The pellet containing the mitochondria was suspended with 0.5-1 mL of HB buffer depending on the pellet's size and frozen at -80 $^{\circ}$C for future use. Protein concentration was calculated using a DC™ BioRad protein concentration assay kit (Hercules, CA) according to the provided instructions. All centrifugation steps were done in a Beckman Coulter microfuge model 20R.

Western Blotting:

Ten micrograms of protein were treated with 2X SDS sample buffer (Sigma-Aldrich, St.Louis, MO) and left to incubate at 95°C for 5 minutes. The samples were loaded on a 3-12%

denaturing SDS polyacrylamide gel (Thermofisher Scientific. Waltham, MA), and run at constant voltage of 80V for 45 minutes at room temperature. Voltage was increased to 120V once the samples had traveled halfway down the gel. The gel was transferred to a nitrocellulose membrane (Bio-Rad, Hercules, CA) for 35 min at an amperage of 300 mA. The membrane was treated for 1 hour submerged in 10% dry milk in phosphate buffered saline, pH 7.4 containing 5% tween 20 (PBST) at room temperature, and then washed with PBST three times for 5 min each at room temperature. The membrane was then incubated with a primary antibody (see Table 1) in 1% milk in PBST for 1 hr at room temperature, washed three times with PBST for 5 min each at room temperature, then incubated with a dilution of 1:3000 donkey anti-rabbit, alkaline phosphatase (AP) secondary antibody (Bio-Rad, Hercules, CA) in 1% milk in PBST for 1 hour at room temperature. The membrane was washed three times with PBST for 5 min each, and then left in 1-step developer (Thermo Fisher Scientific, Waltham, MA) for 15-30 minutes until bands became visible. Band position and relative intensity were quantitated with NIH ImageJ software.

Table 1. Antibodies used for Western blotting

Antigen	Source	Dilution	Clonality
ACAD9	Rabbit	1:1000	Polyclonal
VLCAD	Rabbit	1:1000	Monoclonal
ECSIT	Rabbit	1:500	Polyclonal

Blue Native Gel Electrophoresis:

A 1:5 master mix of digitonin:HEPES (Millipore. Burlington, MA) was made and incubated at 95 °C for 5 min to dissolve into solution. The digitonin mixture was placed on ice for at least 20 min then added to mouse mitochondria samples to give a 1:5 ratio of

protein:digitonin and a 3 mg/mL protein concentration. The samples were incubated on ice for an additional 30 min, then Coomassie blue stain (0.1% R250, BioRad) in 7% acetic acid, 40% methanol in water was added at a dilution between 1:20 – 1:30 and re-suspended by pipette. Samples were centrifuged at 17,000 rpm for 1 hr at 4 °C. The supernatants were transferred to new vials carefully so as to not disturb the pellets then loaded onto a 3-12%, 10-well bis-tris gel (Native-PAGE; Thermo Fisher Scientific, Waltham, MA). The gel was run at 80V for 4-5 hours at 4ºC, then stained with Coomassie R_{250} stain for 15 min, and de-stained for 30 minutes to 1 hour or until the stain is sufficiently removed in 10% acetic acid, 40% methanol mixture in water.

Magnetic Resonance Imaging (MRI) of Mouse Heart Structure and Activity:

MRI imaging of mice was performed in the UPMC Children's Hospital Animal Imaging Core under isoflurane anesthesia according to their standard protocol using a 7T micro magnetic resonance imaging system (Bruker micro-MRI, BioSpin 70/30). Scanning time for each mouse was between 20-45 minutes. Afterwards the mouse was placed in a separate cage with a heating lamp until it regained consciousness and was returned to its original cage.

Hanging Wire Test:

A custom hanging wire apparatus was constructed from standard household software (pictured below). Before the trial, each mouse started with a fall score defined as 10. The mouse was lowered onto the middle of the wire and allowed to hang by its front paws. The mouse was released, and a timer for 180 seconds was started. If the mouse fell, the timer was immediately stopped, the mouse's fall score was reduced by one, the mouse was placed back on the center of

the wire, and the timer was restarted. If the mouse reached either end of the wire, the timer was stopped, the mouse was placed back on the center of the wire, and the timer was restarted again. This continued for 180 secs or until the mouse's fall score reached zero. Fall score, and elapsed time were recorded. Each 180-second trial was repeated consecutively, in triplicate for each mouse.

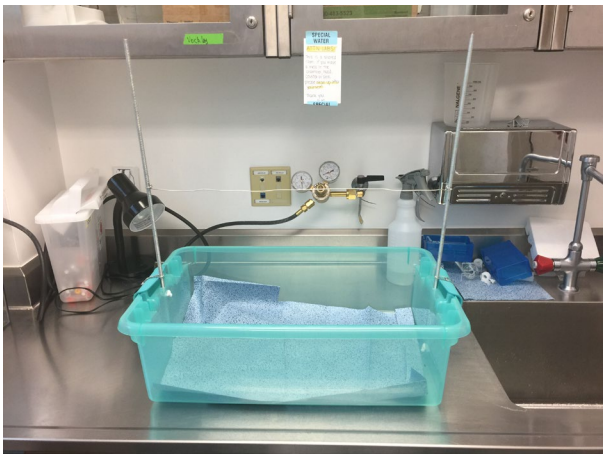

Figure 9 Hanging wire apparatus, constructed from common household hardware

Measurement of Blood Glucose and L-Lactate:

A drop of blood was extracted from the mice by making a small incision near the tip of the tail using a small pair of surgical scissors. The directions of the glucometer (AimStrip Plus. Thermo Fisher Scientific, Waltham, MA) and strips and L-lactometer (Lactate Scout. EKF Diagnostics, Elkhart, IN) and strips were followed to measure each parameter. Bleeding was halted using Kwik Stop (ARC Laboratories, Dayton, OH). Glucose and lactate were measured before and after the hanging wire test.

Administering tamoxifen to Induce Cre-ER in Mice:

Mice were provided tamoxifen-containing food (Envigo. Huntingdon, United Kingdom) (500 mg/kg) in place of standard mouse food and monitored for any significant weight loss associated with tamoxifen ingestion.

Measuring ROS of WBC from Whole Blood Sample:

MitoSOX, and LD/CD45 stains (San Jose, CA) were freshly prepared before each experiment according to the manufacturers' instructions. A mouse blood sample was extracted by making a small incision near the tip of the tail and siphoned off into an Eppendorf tube. Bleeding was stopped using Kwik Stop™. Blood was incubated at 37 °C with both stains for 10 minutes and then sorted using flow cytometry for viability, CD45 antigen (WBC vs. RBC), and MitoSOX level.

Immunofluorescence Staining of Paraffin-Embedded Tissues:

Slides containing paraffin-embedded tissues were washed several times with xylene to remove wax from the samples, rehydrated with a series of washes of ethanol (100, 70, 50%), and finally washed in PBS. Slides were incubated in sodium citrate buffer (10 mM, 6.0 pH) starting at 37 °C increasing to 95 °C over 20-30 min, then held there for 20 minutes. After incubation, the slides were left to cool, the buffer was removed, and the slides were washed with PBS. Slides were incubated with 0.1% Triton X-100 in PBS for 10 minutes in order to permeabilize the cells, washed with PBS, then transferred to a hydrated incubation chamber to prevent desiccation. Using a PAP (Peroxidase Antiperoxidase, Thermofisher Scientific, Fremont, CA) hydrophobic pen, each samples was circled in order to hold staining solutions in place, then incubated with a

series of hour-long, room temperature stains beginning with blocking buffer (5% donkey serum in PBS), the primary antibodies of interest, then secondary, anti-rabbit fluorescent antibody, washing with PBS in between each step. After the final wash, the DAPI counterstain was applied and left to incubate for 5 minutes. A drop of mountant permafluor (Thermofisher Scientific, Fremont, CA) was applied to each sample, a coverslip was placed over each sample and sealed with clear nail polish, left to dry for 2 hours, and finally stored at -20°C until visualization.

2.3 Specific Aim 1: Results

2.3.1 Specific Aim 1a

2.3.1.1 Heart Tissue-Specific ACAD9 Deficiency Results in Viable Birth, but is Lethal Within 27 Days.

The first litter from a breeding between a mouse heterozygous for the floxed *Acad9* allele and *Cre* under the control of a cardiac specific alpha myosin heavy chain promotor and a mouse homozygous for the floxed *Acad9* allele yielded four offspring in the expected 1:1:1:1 ratio of possible genotypes (Cre+;Homozygous Floxed : Cre+;Heterozygous Floxed : Cre-;Homozygous Floxed : Cre-;Heterozygous Floxed). Homozygous *Acad9* deficient offspring had lifespans ranging from 13 to 27 days. To allow clinical phenotyping, offspring were genotyped immediately after birth so that results could be ready by day postnatal 3 (P3). Subsequent crosses showed similar ratios of genotypes.

2.3.1.2 MRI's of Heart-Specific ACAD9 Deficient Mice Show Evidence of Cardiomyopathy Consistent with the Human Phenotype.

To characterize the cardiac phenotype of mutant mice, cardiac MRI's were performed at age p14 as they began to die thereafter (earliest death was p13). Mutant animals exhibited dramatic cardiomyopathy as seen in ACAD9 human patients. Hearts of affected animals exhibited noticeable thickening of the atrial and ventricular walls, and all chambers showed severe enlargement (Figures 9-11). The ejection fraction of affected hearts (a measure of dynamic blood flow) was also dramatically reduced in the mutant mice by as much as 27-fold. (Figure 12).

2.3.1.3 Age of Onset of Cardiomyopathy in Cardiac Tissue Specific Mutants

MRIs of animals at day p3 already showed significant cardiomyopathy and reduced ejection fraction (Figures 13 and 14). These findings suggest that the cardiomyopathy began *in utero* rather than after birth. Unfortunately, prenatal echocardiography was not available to examine heart function *in utero*.

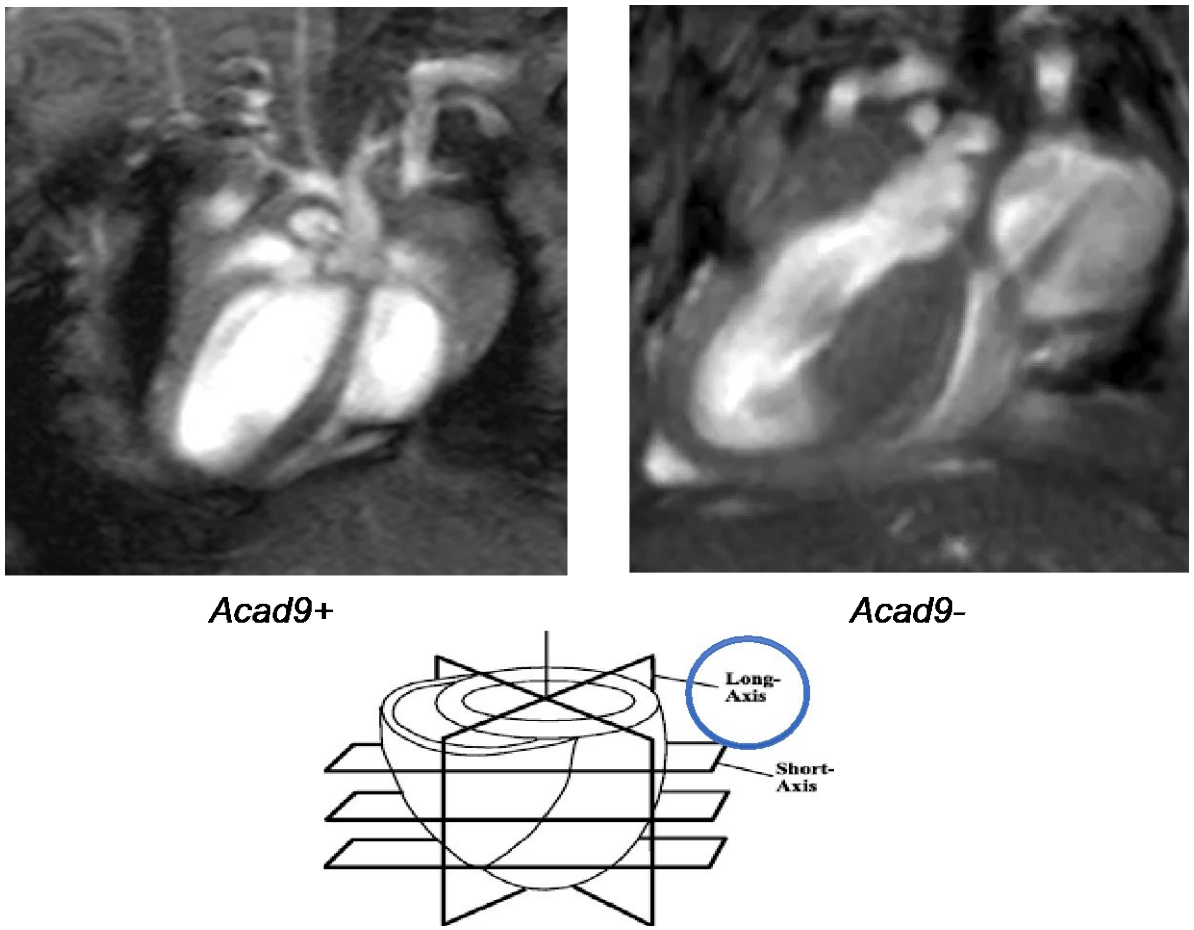

Figure 10 MRI of p14 Mouse Hearts at Long-Axis 4-Chamber Orientation

On the left is a wild type littermate with a normal phenotype. The right image is an ACAD9 deficient mouse heart with thickened ventricular walls, and reduced ejection fraction. These symptoms are also visible from other orientations as seen in Figures 10 and 11. Video can be found at https://pitt.box.com/s/jpej8kxhvnetst7p6uhpvhfc36sz21s2.

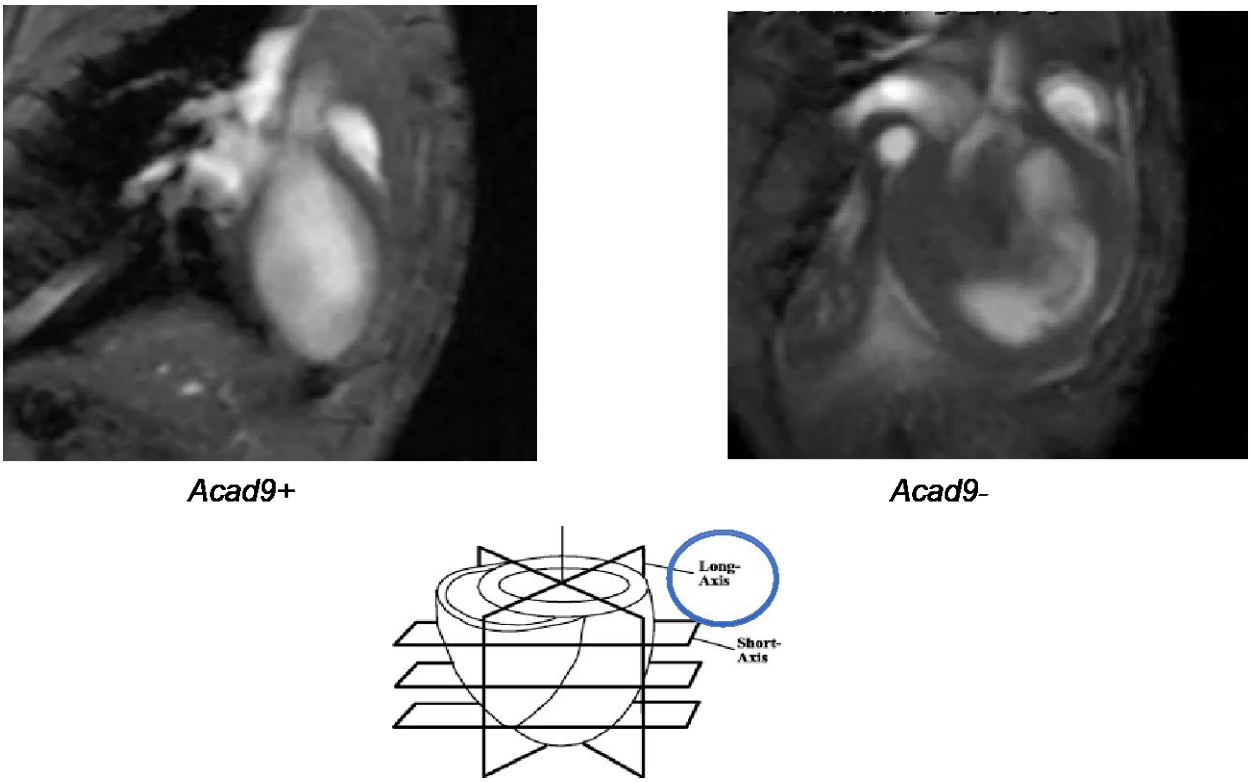

Figure 11 MRI of p14 Mouse Hearts at Long-Axis 2-Chamber Orientation

Cardiac pathology is evident in mutant animals (right panel) compared to wild type (left panel). Video can be found at https://pitt.box.com/s/jpej8kxhvnetst7p6uhpvhfc36sz21s2.

Cardiac ejection fractions were calculated by determining the difference in surface area of the visible blood in the left ventricle at its largest and smallest. Ejection fractions showed a nearly 27-fold difference between the mutant and wild type mouse (Figure 12).

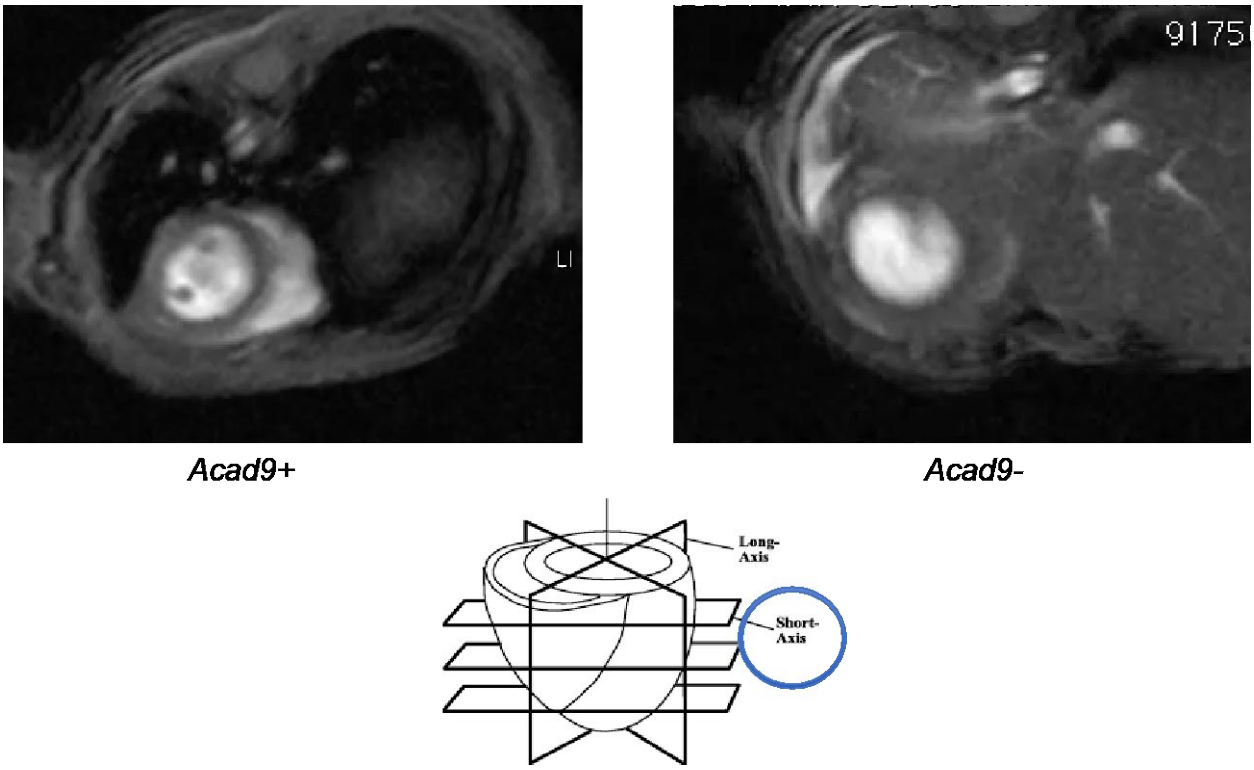

Figure 12 MRI of p14 Mouse Hearts at Short-Axis Orientation

Cardiac pathology is evident in mutant animals (right panel) compared to wild type (left panel). Video can be found at https://pitt.box.com/s/jpej8kxhvnetst7p6uhpvhfc36sz21s2

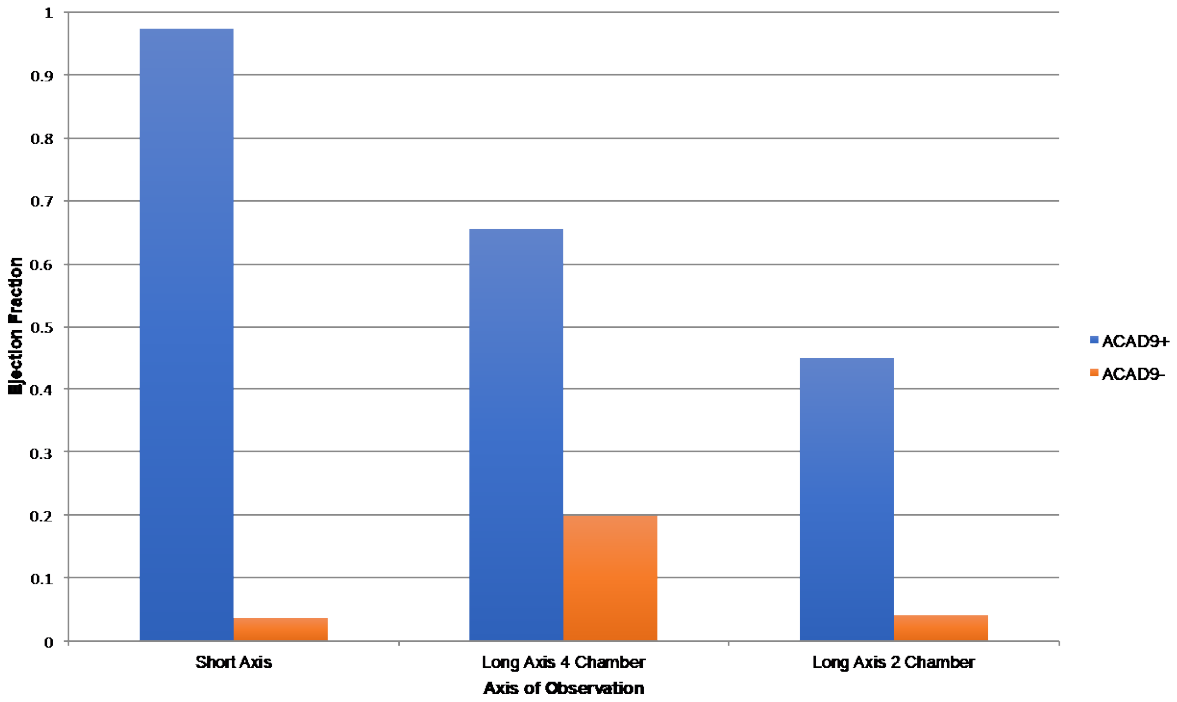

Figure 13 Comparison of Ejection Fraction Between a Single ACAD9D Mouse and WT Littermate

Cardiac ejection fractions calculated using all three orientations. Ejection fractions were calculated by determining the difference in surface area of the visible blood in the left ventricle when it is at its largest and smallest (i.e. an image where the left ventricle completely closes would have an ejection fraction of 1. Data was extrapolated from a single mouse whose MRI data is visible in figures 9-11.

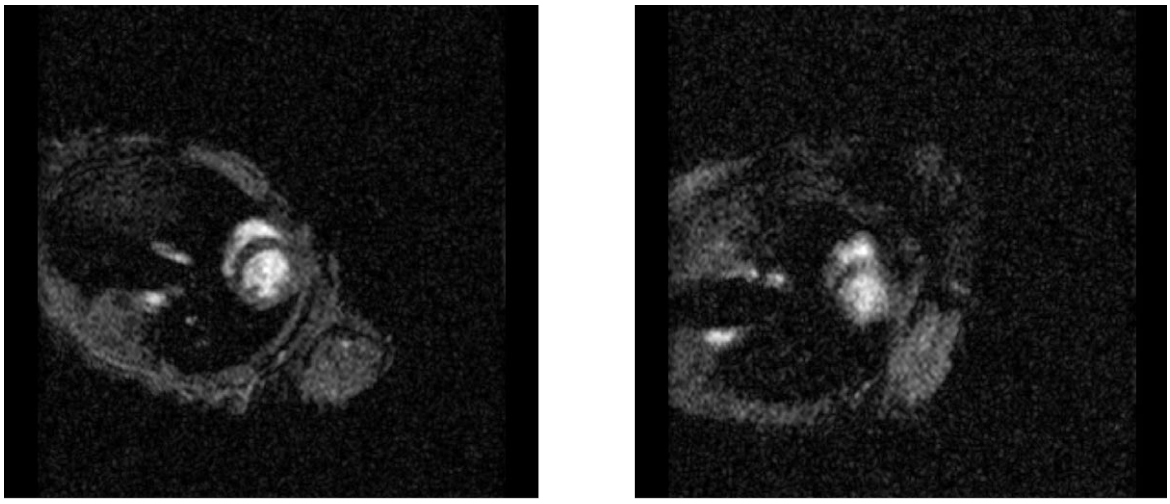

Acad9+ *Acad9-*

Figure 14 MRI of p3 Mouse Pups at Short-Axis Orientation

While the still images appear much less dramatic than their p14 counterparts, the videos show a reduced performance on the part of mutant heart as evidenced by the calculated ejection fractions shown in Figure 12. Video can be found at https://pitt.box.com/s/jpej8kxhvnetst7p6uhpvhfc36sz21s2.

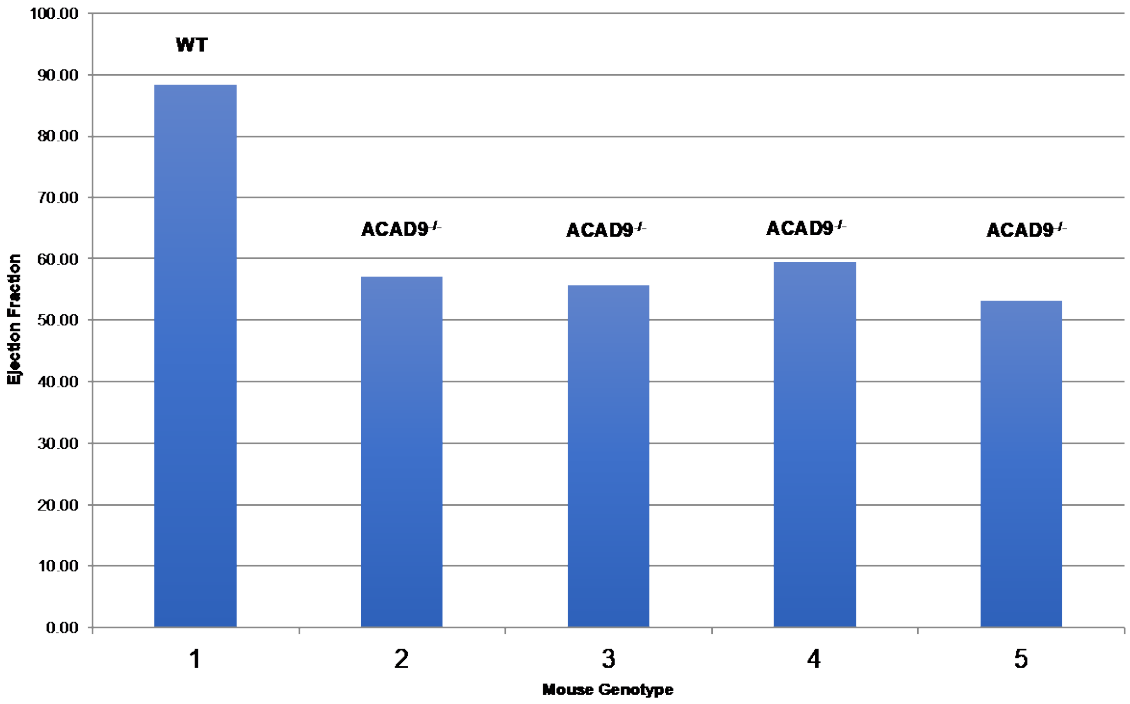

Figure 15 Ejection Fraction of p3 Mice Hearts

Ejection fraction measured at day p3 is significantly decreased in mutant animals (2-5) compared to wild type (1) suggesting that the pathologic process started *in utero.* Ejection fraction was measured from the short axis in four ACAD9D mice and one wildtype littermate.

2.3.1.4 Tissue Immunohistochemistry and Protein Analysis of ACAD9 Mice

Immediately after MRI analysis at p12, heart tissue was harvested from mutant animals and processed for histologic and molecular analysis. H&E stain showed morphological changes consistent with cardiomyopathy seen in human ACAD9 deficiency (Figure 15). Specifically, cells show a disorganized morphology different from the normally, striated muscle pattern seen in healthy cardiac tissue. Immunohistochemistry analysis of wild type tissue stained with ACAD9 and antibodies to NDUFV1, a complex I protein, showed colocalization of both proteins to the mitochondria (yellow merged signal in Figure 16). Western blotting of extracts from flash frozen hearts confirmed that ACAD9 levels were reduced in mutant animals when compared to

phenotypically normal littermates (Figure 17). Finally, BNGE confirmed that isolated complex I and ETC supercomplexes were missing in cardiac tissue of mutant mice compared to wild type (Figure 18).

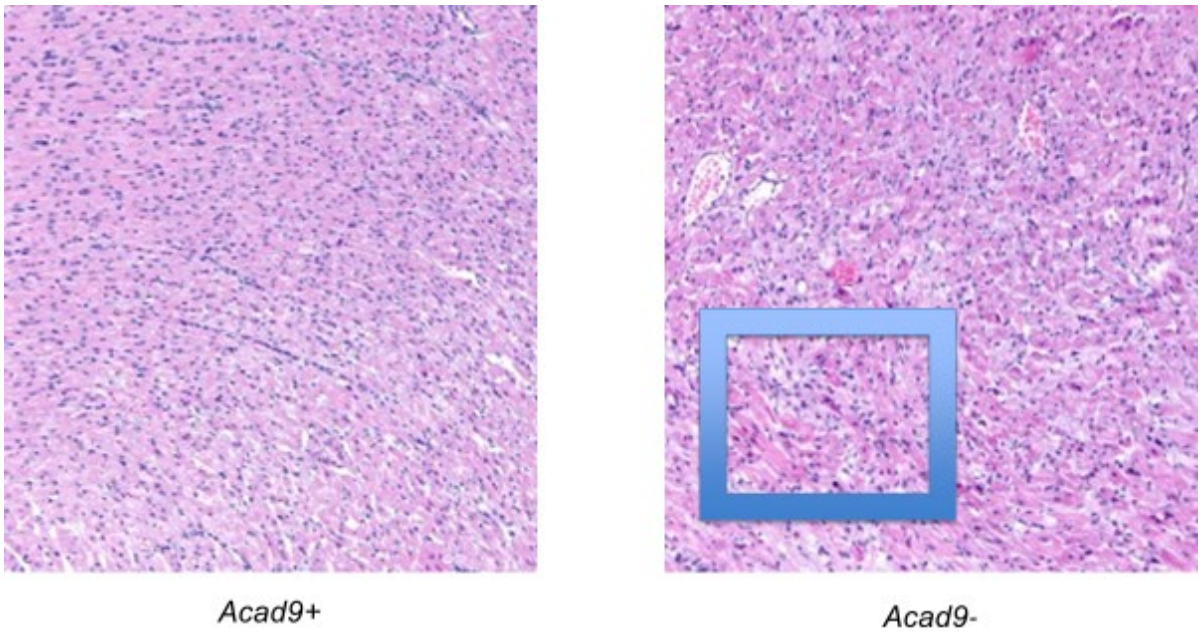

Figure 16 H&E Stains of Mouse Cardiac Tissue (10X)

Acad9 deficient tissue (right panel) shows distinctive disorganized morphology characteristic of cardiomyopathy as compared to the striated and organized orientation of the cardiac cells in the wild type littermate (left panel). This is seen prominently in the swirled patterns and clustered nuclei of the cells (highlighted in the square).

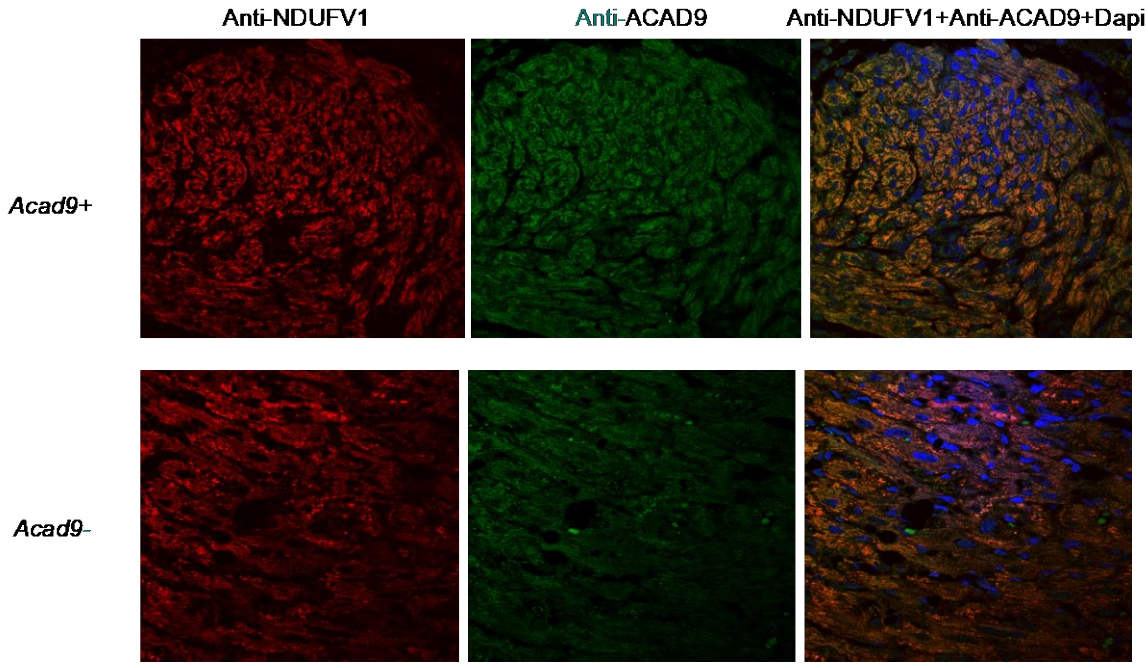

Figure 17 Immunohistochemistry Stains of Cardiac Tissue-Specfic Acad9 Mouse Cardiac Tissue (40X)

Cardiac tissue from wild type (top) and mutant (bottom animals) were stained with NDUFV1 antibody (left panel) and visualized with a red fluorescently labeled second antibody; ACAD9 body (center panel) visualized with a green fluorescently labeled second antibody; The two images are shown merged (right panel) with yellow representing overlapping signals. The nuclear stain DAPI is shown in blue in the right panel.

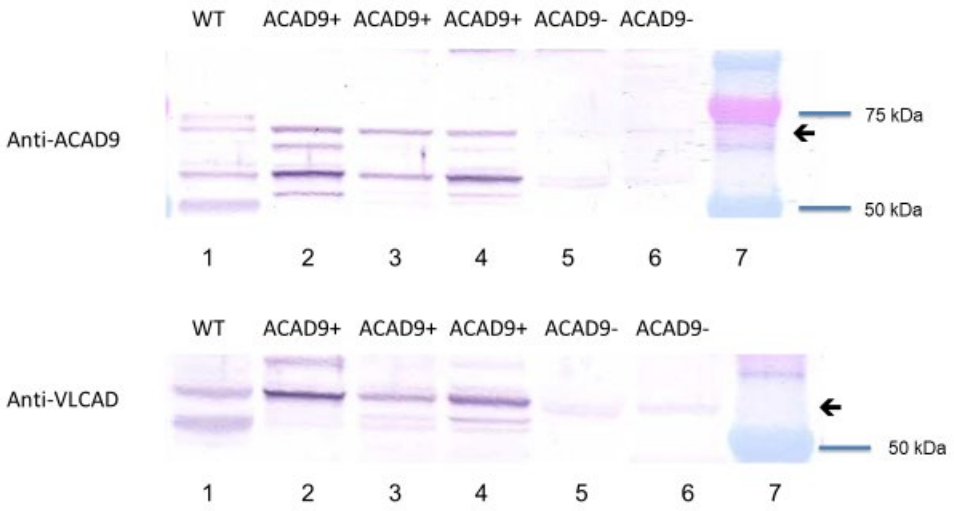

Figure 18 Western Blots of Homogenized ACAD9D Mouse Cardiac Tissue

Heart extracts from wild type and mutant animals were separated on SDS-PAGE gels, transferred to a membrane, then analyzed by western blotting. The top panel shows staining of the membrane with ACAD9 antibodies (top panel. A VLCAD antibody was used as a positive control (bottom panel). The molecular mass of the two proteins are 62 kDa (VLCAD) and 68 kDa (ACAD9).

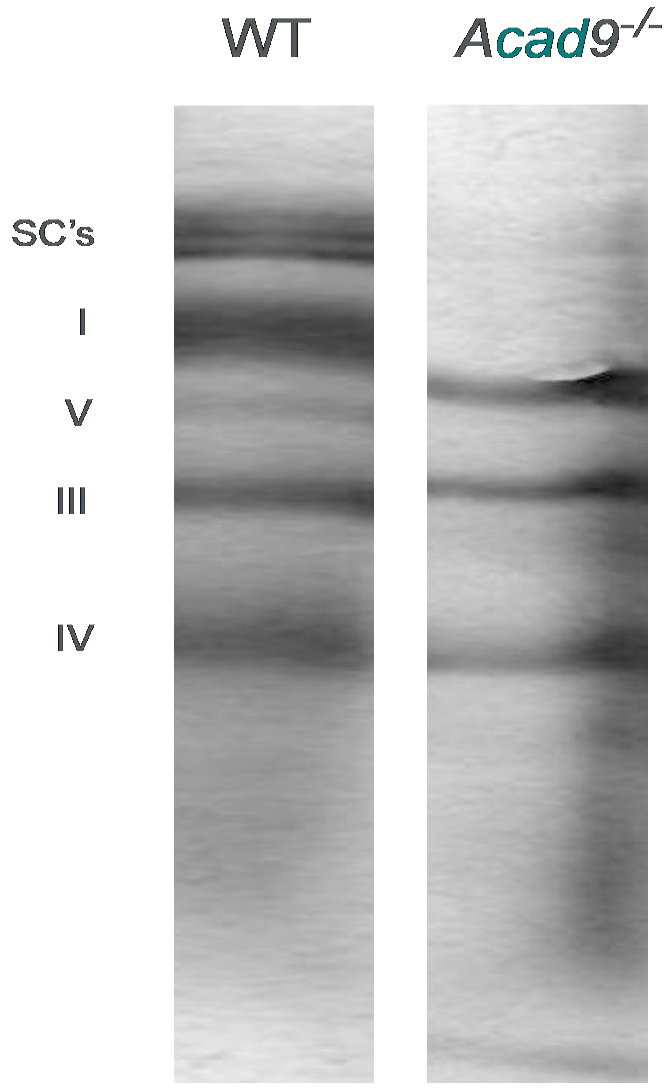

Figure 19 Blue-Native Gel Electrophoresis of Cardiac Tissue Mitochondria from ACAD9D and Wild Type Animals

Extracts from wild type (left panel) and mutant (right panel) animal hearts were separated by BNGE and stained with Coomasie Blue. The known migration positions of ETC complexes are indicated on the left. Supercomplexes (SC) consist of various combinations of complex I, III, and IV, and are absent in mutant animals, as is isolated complex I.

2.3.2 Specific Aim 1b

2.3.2.1 Skeletal Muscle Tissue-Specific ACAD9 Deficient Mice Show a Myopathy

Mice homozygous for the floxed allele of *Acad9* were bred with mice homozygous for the floxed allele and heterozygous for a human alpha-skeletal actin promoter-linked Cre driven allele. Matings gave the expected number of animals, 42 Cre negative and 39 Cre positive mice. This suggests a lack of *in utero* lethality. Molecular analysis of tail snip DNA identified 1:1 ratio for pups containing the *Cre* allele and those without. All mice were viable and survived to adulthood. At 2-6 months of age mice were subjected to the hanging wire test and their fall scores and times of each fall were recorded to create a Kaplan-Meier-like survival curve (Figure 19). All mutant animals demonstrated an inability to complete the test as compared to the wild type animal, indicating a loss of exercise tolerance.

Mice were examined for changes in blood glucose and L-lactate levels before and after the hanging wire test. Blood was taken from small tail incisions and the glucose and lactate concentration was measured as described in the methods. ACAD9 skeletal muscle deficient mice had elevated lactate levels at baseline and developed an exaggerated increase L-lactate during the wire hang test compared to wild type animals (Figure 20).

Skeletal muscle tissue acquired after the test was stained and analyzed for the presence of ACAD9 as well as for morphological condition of the structure of the tissue. Both western blotting of the mitochondria extracted from the muscle tissue, as well as immunohistochemical staining of slides of skeletal muscle tissue confirmed the absence of ACAD9 within the affected tissue (Figures 21 and 22). H&E and trichrome staining like-wise, demonstrated morphological aberrations such as nuclear clumping consistent with diagnoses of muscular myopathy (Figures 23A and 23B).

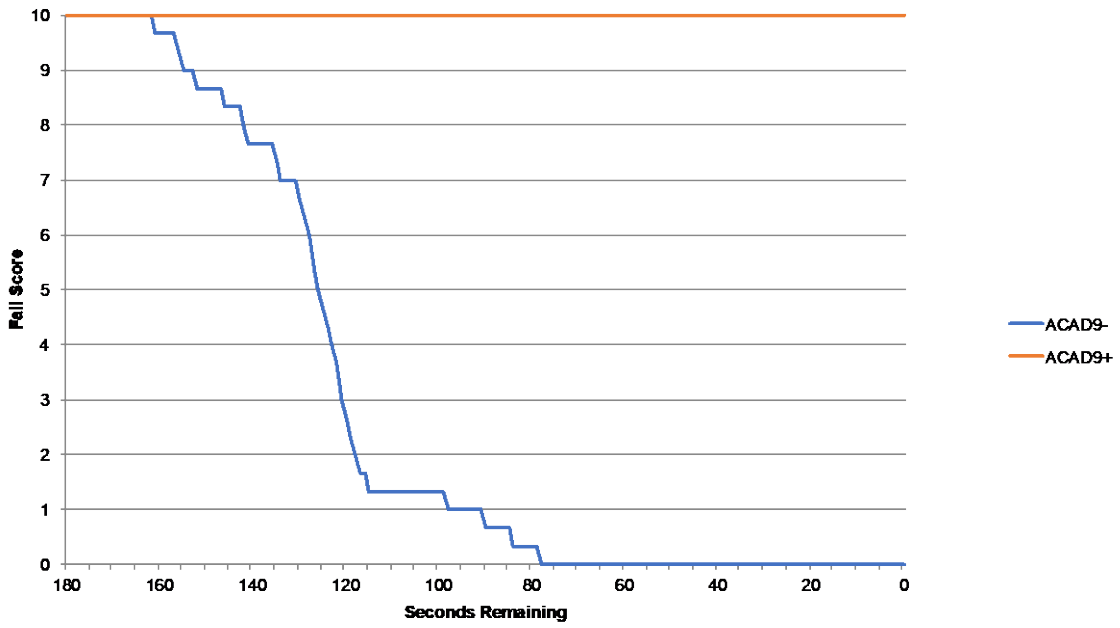

Figure 20 Kaplan-Meier-Like Curve Measuring Fall Score of ACAD9D Skeletal Muscle-Specfic Mice

Average of fall scores over a period of 180 seconds. While all normal mice were able to last the full three minutes, All mutants had received a final fall score of zero by 78 seconds. Data represents 1 ACAD9+ and 3 ACAD9- mice.

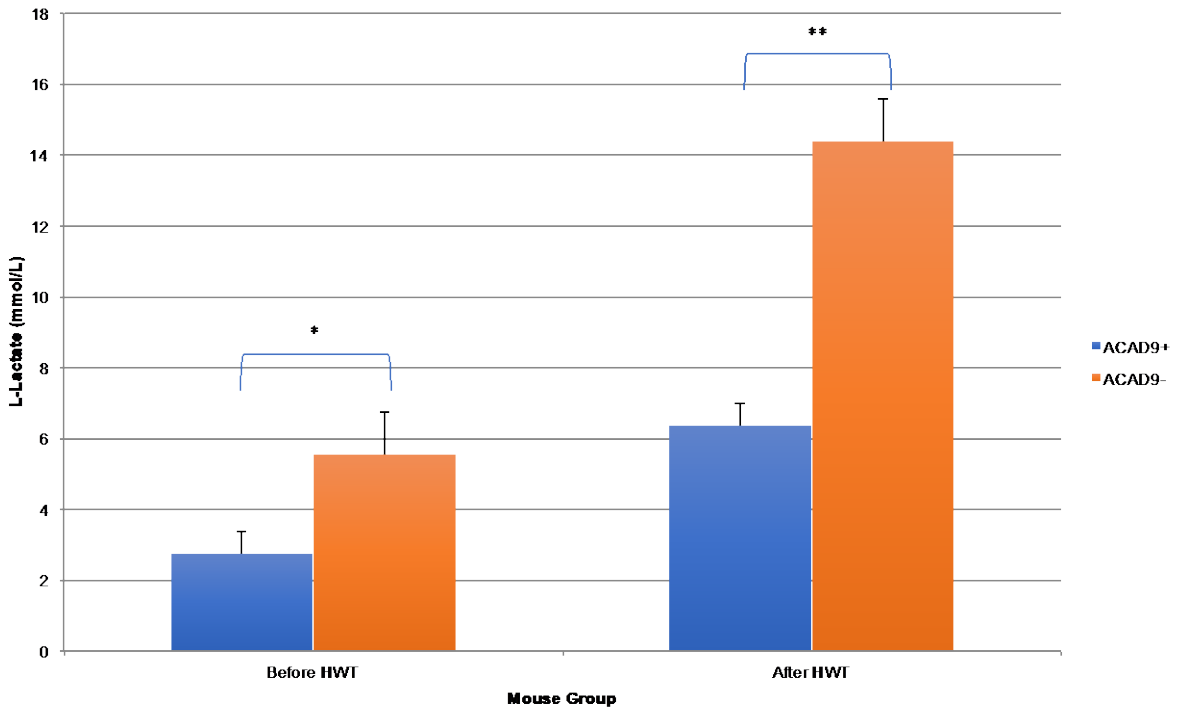

Figure 21 Blood L-Lactate Levels in Skeletal Muscle-Specfic ACAD9 Deficient Mice Taken Before and After a Hanging Wire Test

Muscle ACAD9 deficient mice have an increased resting L-Lactate levels compared to wild type littermates (blue), which increases more than wild type following exercise (red; the hanging wire test). *p-value = 0.002, **p-value = 0.004.

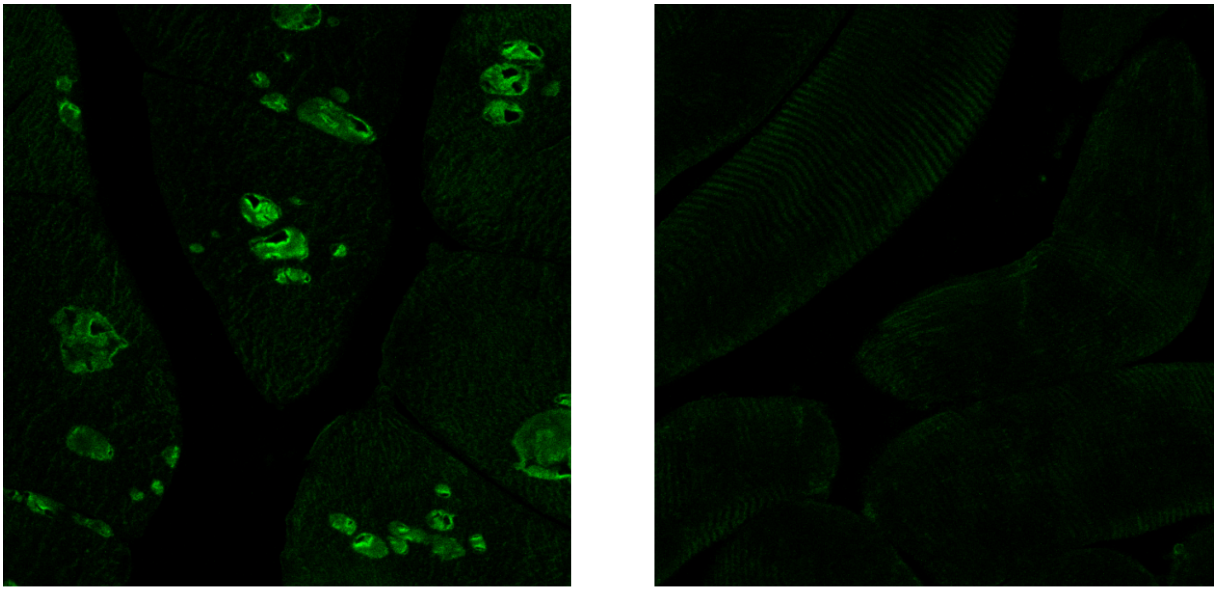

Figure 22 Immunohistochemistry Stains of Skeletal Muscle-Specfic ACAD9D Mouse Muscle Tissue with ACAD9 Antibody

Wild type skeletal muscle stains brightly (green) with ACAD9 antibodies (left panel), while no signal was evident in mutant mice (right) Magnification was 10X.

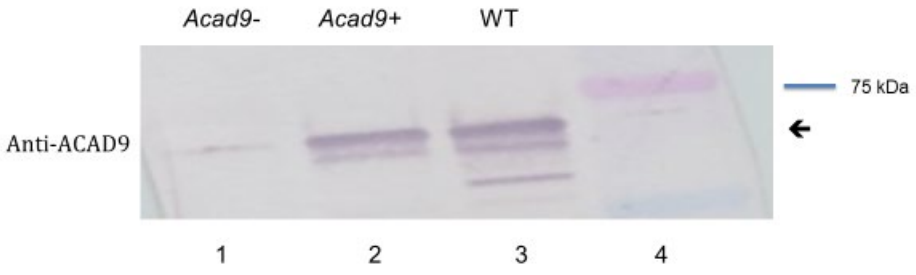

Figure 23 Western Blot of ACAD9D Skeletal Muscle Mitochondria Using ACAD9 Antiserum

The ACAD9 deficient mouse shows no signal with ACAD9 antibody in contrast to the *Acad9+* littermate. The arrow indicates 68 kDa.

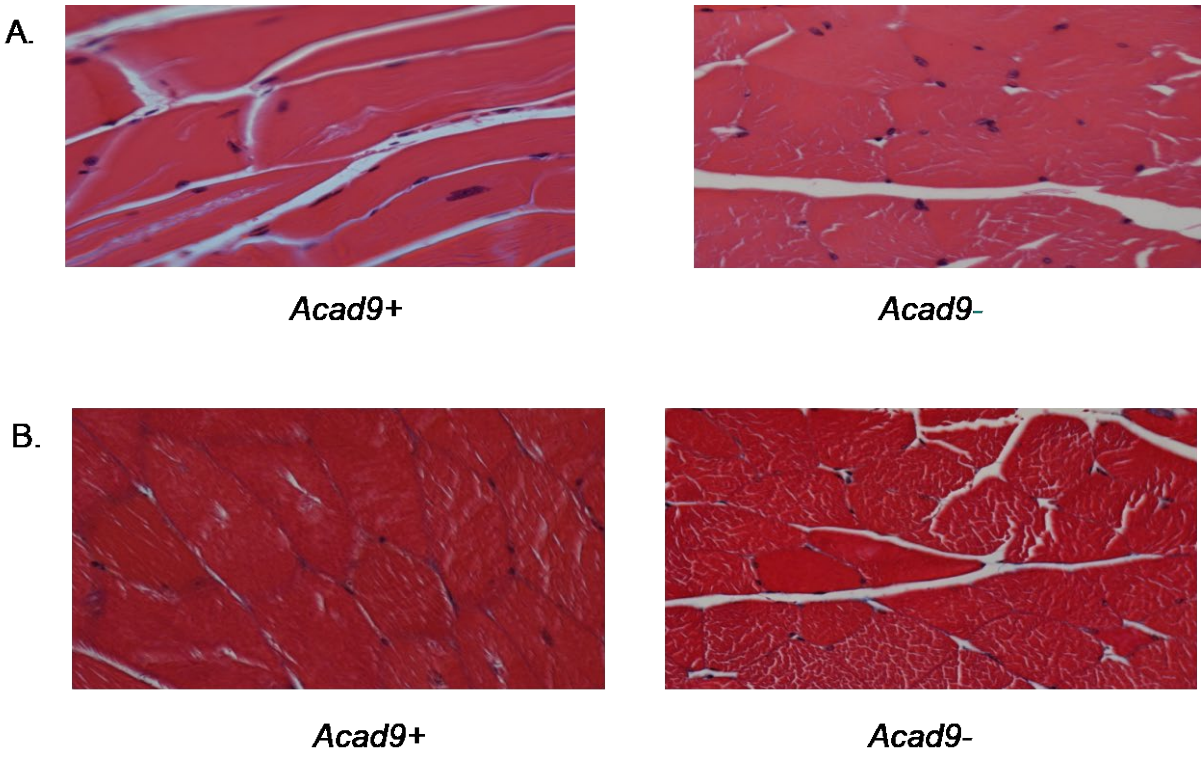

Figure 24 H&E (A) and Trichrome Stain (B) of Skeletal Muscle-Specfic ACAD9D Mouse Muscle Tissue

Normal muscle morphology is present in wild type animals (left panel). ACAD9 deficient animals show disruption of the normal myofibril bundles and centralized nuclei suggestive of chronic muscle damage. The trichrome staining of skeletal muscle tissue highlights the more disorganized morphology of the ACAD9 deficient muscle as compared to the more striated pattern of the phenotypically normal littermate Magnification is 40X.

2.3.3 Specific Aim 1c

2.3.3.1 Induction of a Ubiquitously Expressed Cre Gene

Homozygous, floxed *Acad9* mice were bred with mice with a single copy of *Cre* driven by the human ubiquitin C Cre-linked human estrogen receptor (UBC-Cre-ERT2). Mice are heterozygous for the *Cre-ERT2* allele express Cre when administered tamoxifen. This method should allow creation of mice deleted of the *Acad9* gene in all tissues following initiation of induction with tamoxifen. Three months after induction, six mice (three each Cre positive and negative) were subjected to the hanging wire test on weekly intervals to observe any change in exercise tolerance. After 6 months of continual induction, no change was observed (Figure 24).

After more than six months of induction, tail snips were taken for western blotting, which did not reveal a reduction of ACAD9 protein (Figure 25). Whole blood samples treated with MitoSox and analyzed by flow cytometry showed an increased signal in white blood cells compared to the wild type, indicating increased mitochondrial stress (Figure 26). However, histologic staining of muscle tissue from animals after six months after induction showed relatively normal architecture (Figures 27A and 27B), as did all other tissues including heart (not shown). Finally, cardiac MRIs were normal in mutant animals (Figure 28).

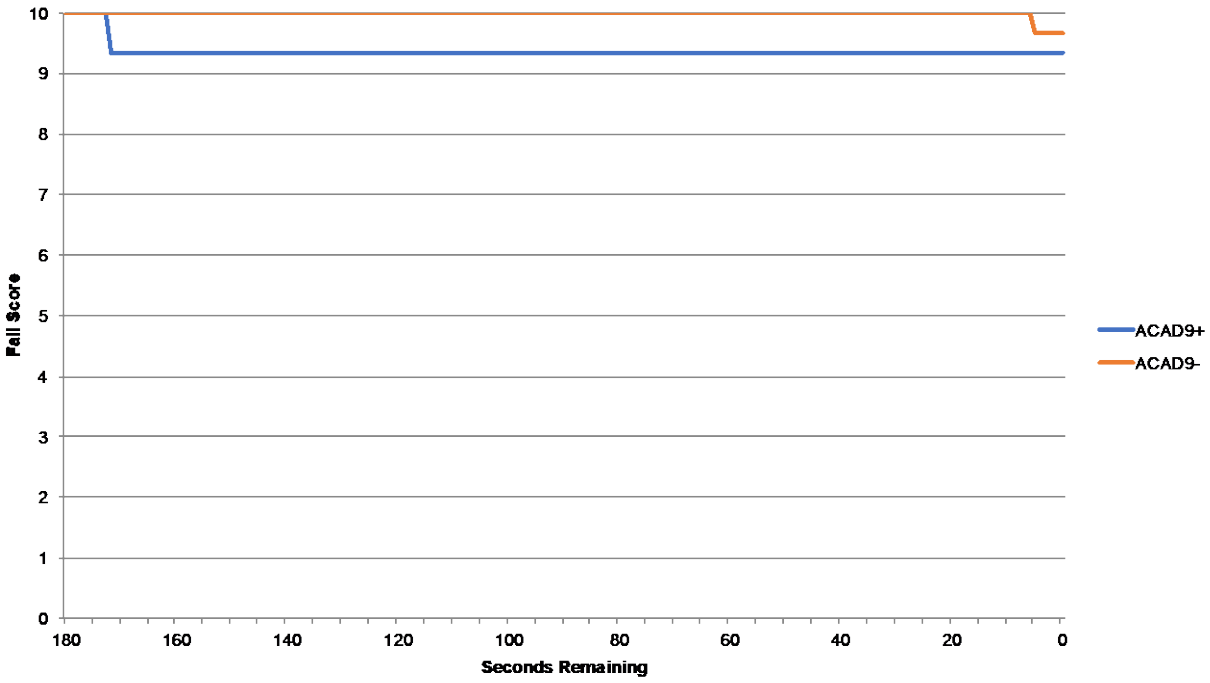

Figure 25 Hanging Wire Test of Induced Whole Body Induced ACAD9D Mice

After six month of induction with Tamoxifen, the mice were given the exercise test. Differences in the mice's capability to stay on the wire for 180 seconds was negligible. Both the ACAD9+ and ACAD9- groups contained 3 mice each.

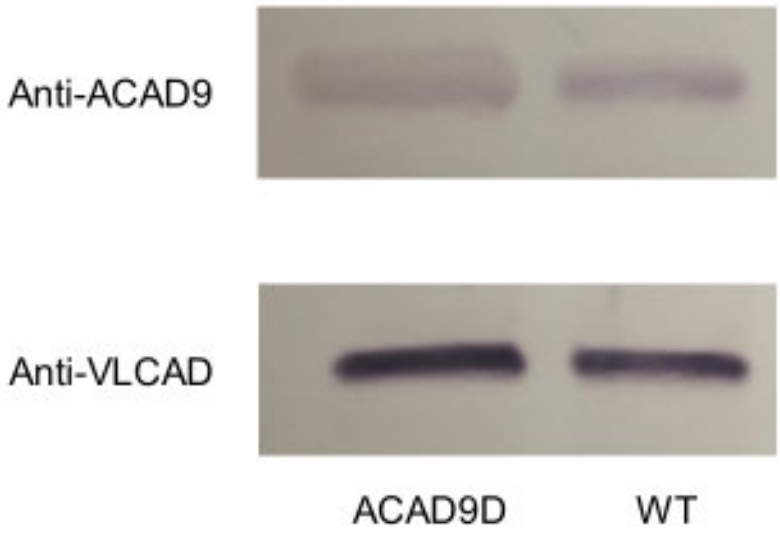

Figure 26 Western Blot of ACAD9 in Ubiquitously Induced Acad9 Knockout Mice

Protein was extracted from mitochondria in heart tissue from both phenotypically normal and induced ACAD9 deficient mice. Protein was stained with antisera for VLCAD (positive control), and ACAD9. These blots suggest no change in ACAD9 expression between the two mouse types.

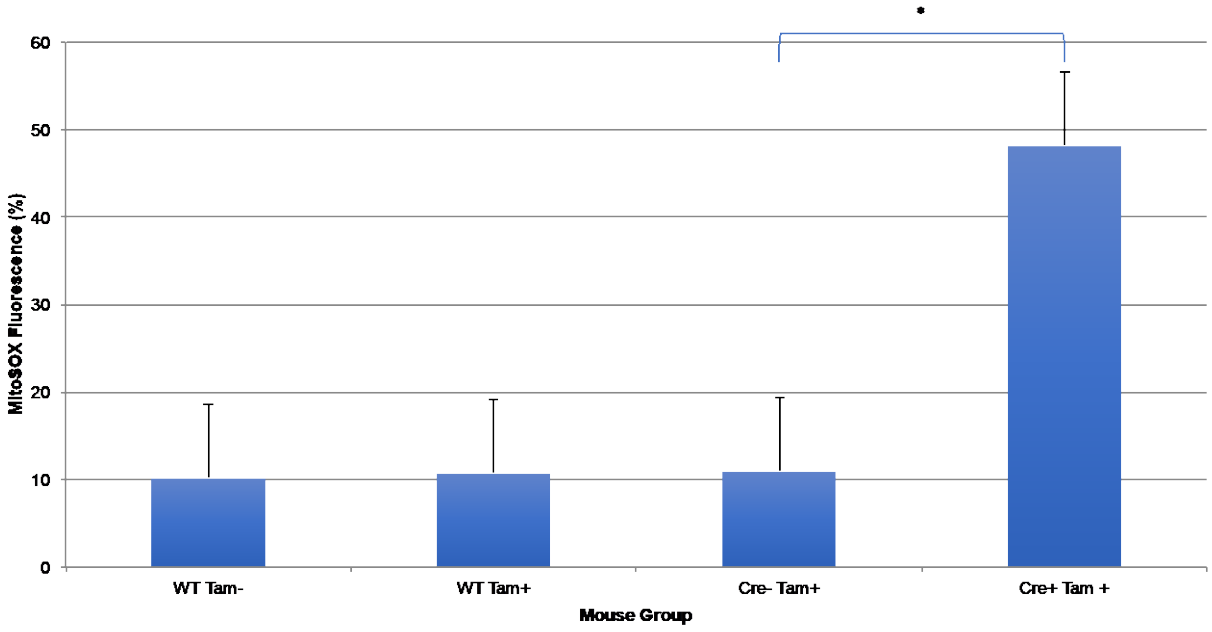

Figure 27 Superoxide Accumulation in WBCs from Whole Body Induced ACAD9D Mice

White blood cell samples were obtained, treated with MitoSox, and analyzed by flow cytometry. Each sample group contained 3 mice. Error bars indicate one standard deviation. *p-value = 0.0028.

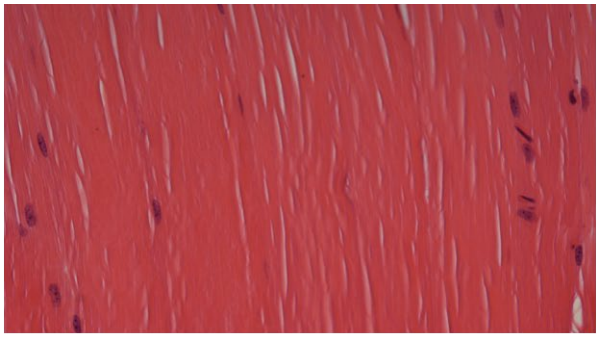

Acad9+

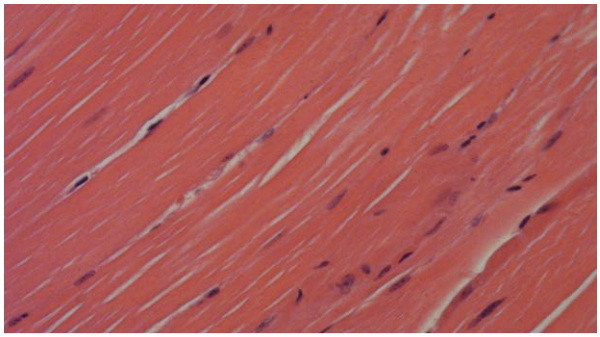

Induced *Acad9-*

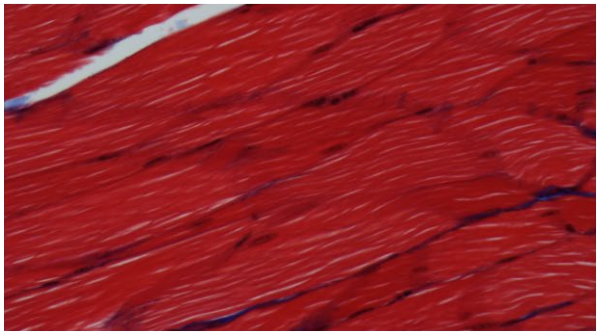

Acad9+

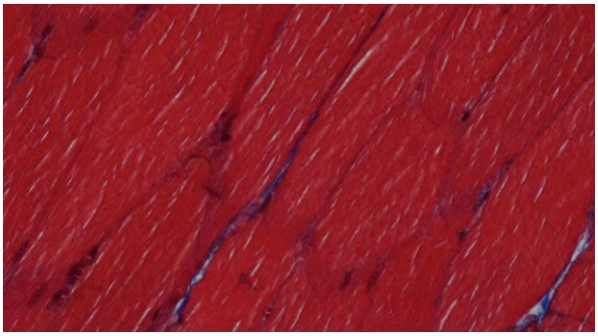

Induced *Acad9-*

Figure 28 H+E Staining (A) and Trichrome Staining (B) of Skeletal Muscle Tissue of Ubiquitously Induced Acad9 Knockout Mice

After six months of induction with Tamoxifen, skeletal muscle tissue was harvested and stained with H&E and trichrome. Muscle cell structure was unaffected after 6 months of treatment. Images were taken at 40X magnification.

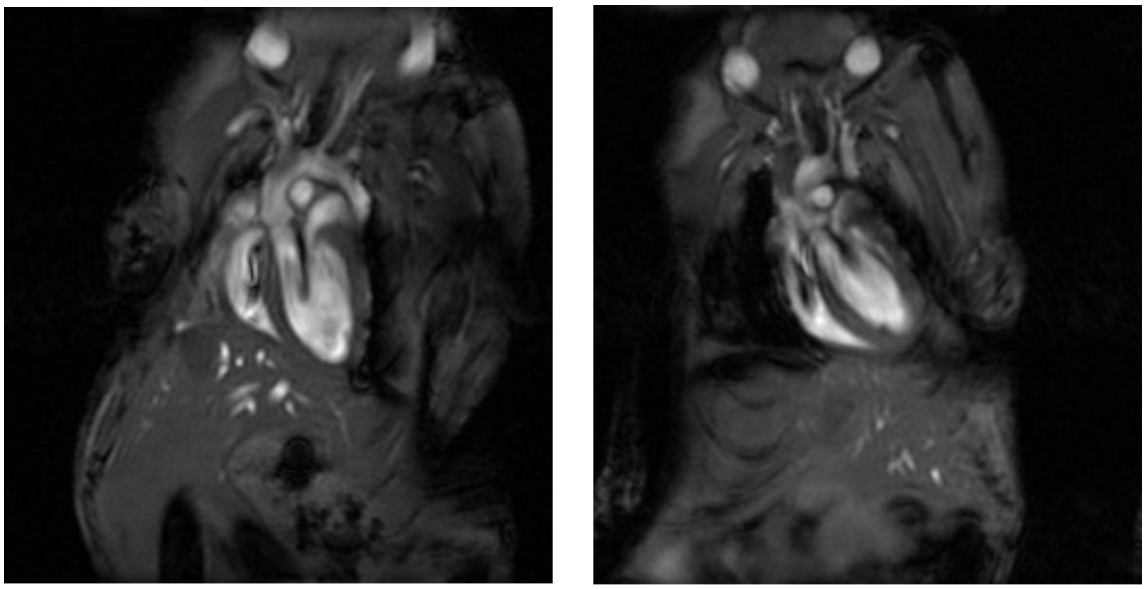

Figure 29 MRIs of Ubiquitously Induced ACAD9D Mice

After over six months of induction of Cre, MRI's of the heart show no morphological different between the ACAD9 deficient hearts and the non-induced mice. Ejections fractions were identical (not shown).

2.4 Specific Aim 1: Discussion

ACAD9 Deficiency is the most commonly recognized cause of isolated ETC complex I deficiency and can present in infancy with severe systemic lactic acidosis, cardiomyopathy, and early death. However, later presentations are common, predominantly with cardiomyopathy and milder symptoms that are sometimes responsive to riboflavin supplementation. The first attempt to study this disease in a whole body knock out mouse was unsuccessful due to lethality in embryogenesis. To circumvent this problem, I elected to construct several tissue and temporal specific knock out models using Cre-lox technology. Prior attempts by the Vockley lab had suggested that complete knock out of ACAD9 was embryonic lethal.

The first model utilized a cardiac muscle tissue specific *Cre* promoter in an attempt to mirror the cardiomyopathy seen in humans. Heart muscle specific ACAD9 deficient mice indeed showed a phenotype consistent with human cardiac pathology, developing severe cardiomyopathy present at the earliest time point examined (p3), suggesting the development of cardiac dysfunction *in utero*. Unfortunately, the animals were quite impaired and died before three weeks of age. Nonetheless, the model successfully demonstrated the expected molecular and biochemical changes, with complete loss of mitochondrial ETC supercomplexes. While the severity of the cardiomyopathy limited the physiologic testing that could be performed, this model will still be valuable for testing therapeutic agents, though *in utero* treatment may be necessary given early onset symptoms. Several possible approaches are available to circumvent the severe disease phenotype. First, an inducible promoter, either cardiac specific or whole body expressible, could be used to create a model with later onset symptoms (see below). Alternatively, a weaker cardiac specific Cre promoter might allow some cells to retain the *Acad9*

gene and thus mitigate the severity of disease. Finally, knocking in a hypomorphic allele into the full body or cardiac specific knock out background could lead to milder symptoms.

To study the myopathy associated with ACAD9 deficiency, a skeletal muscle specific ACAD9 deficient mouse was created next. Unlike the cardiac tissue-specific deficient mice, the skeletal muscle deficient animals were viable and survived to adulthood, allowing direct study of the effect of the ACAD9 deficiency on muscle tissue. Notably, although the mice appeared grossly normal, they demonstrated systemic lactic acidosis and exercise intolerance, making them excellent candidates for therapeutic testing (see Specific Aim 2). The viability of these animals suggests that therapies should target cardiac symptoms in the most severely affected patients in order allow survival to an older age.

Finally, in an attempt to mimic milder, adult disease in humans, I created an animal in which *Acad9* excision was driven by a tamoxifen-inducable Cre promotor at any age. Interestingly, animals allowed to develop to adulthood prior to induction of ACAD9 deficiency had no observable phenotype at the cellular level, with normal ACAD9 protein levels and genotype. Nevertheless, ROS in WBCs from mutant mice was increased compared to those from wild type animals, suggesting some measure of oxidative stress due to otherwise undetected ACAD9 deficiency. There are several possible explanations for this finding. First, the duration of treatment with tamoxifen was insufficient to allow complete deletion of the *ACAD9* gene. This is unlikely given that Cre mediated excision is quite rapid and mice were induced for six months. Second, it may be necessary to start induction earlier than adulthood to allow sufficiently early excision in still developing tissues for the cellular pathology to occur. Treating mice immediately after weaning would allow further evaluation of this possibility. Finally, the level of induction of Cre recombinase from the tamoxifen promotor may not be high enough to produce sufficient

recombinase to efficiently excise the lox targeted *ACAD9* allele. Other inducible Cre promotors are available and can be substituted in future experiments to further explore this possibility.

Ultimately, continued development of these models is worth pursuing as they will provide novel tools to study the interaction of ACAD9 protein with the complex I assembly machinery, the dynamics of ETC supercomplex formation and recycling following loss of ACAD9 function, and therapeutic options to abrogate the effects of ACAD9 deficiency. While the proteins involved with complex I assembly have been identified, the dynamics of their interactions have not. Inducible ACAD9 deficiency in animals or cells would allow characterization of prescribed loss of this protein, while expression experiments adding it back will demonstrate the timing of interaction of the complex I assembly proteins. Similarly, prescribed loss and expression of ACAD9 would provide the opportunity to examine sequential assembly of ETC super complexes, not possible in other current systems. Finally, tissue specific or whole-body inducible models of ACAD9 deficiency provide the rigorous pre-clinical testing of novel therapeutic agents that is necessary to move them to clinical trials in humans, as described in the next Specific Aim.

3.0 Treatment of ACAD9 Deficient Mouse Models

3.1 Introduction

Two groups of ACAD9 deficient patients have been described. One group responds dramatically to riboflavin supplementation, presumed to be due to increased availability of FAD acting as a chaperonin to the maturing enzyme with stabilization of mutant enzymes. The other group of patients do not respond to riboflavin and their treatment is largely supportive, with use of standard medications for cardiac support. Elamipretide is an artificial tetrapeptide that interacts with cardiolipin in the inner mitochondrial membrane and has been shown to increase mitochondrial stability and reduce cellular reactive oxygen in a variety of cellular systems[39]. It is currently in clinical trials for ETC defects including ACAD9 deficiency. Our cardiolipin binding peptide (RTP-03) is an analogue of Elamipretide with similar function but better oral availability. It has not been tested as a potential treatment of ACAD9 deficiency. JP4-039 and XJB-5-131 are antioxidants that target to mitochondria with higher efficiency than other antioxidants routinely used as therapy for ETC deficiency. Both have been shown to reduce mitochondrial superoxide levels in fibroblasts from patients with ACAD9 deficiency and FAO defects[26, 56]. The goal of this specific aim was to test these compounds in muscle specific ACAD9 deficient mice as possible therapeutic agents for this defect in humans.

3.2 Materials and Methods

Materials:

All items were purchased from Millipore Sigma, St. Louis, MO unless otherwise noted.

Treatment of skeletal muscle ACAD9 deficient mice with RTP-03

Thirteen mice (7 wild type and 6 skeletal muscle ACAD9 deficient) were assessed at eight weeks of age with a hanging wire test as described in Specific Aim 1. Weight, blood glucose and L-lactate were measured before and after the test. RTP-03 was prepared freshly before every treatment to a final concentration of 1 mg/mL in PBS and sterilized by filtration. Injections of 2 mg/kg of body weight were administered subcutaneously every 12 hours for a period of two weeks. At the end of two weeks, the hanging wire test was performed again, with weight, glucose, and L-lactate measured before and after the test.

Treatment of skeletal muscle ACAD9 deficient mice with JP4-039.

Twelve mice (7 wild type and 5 skeletal muscle ACAD9 deficient) were assessed with a hanging wire test at eight weeks of age as described above. JP4-039 was dissolved in DMSO to a final concentration of 1 μg/1 μL of DMSO. PBS (1 ml) was added and the mixture was sonicated several times to fully emulsify the solution. Injections of 5 mg/kg of body weight were administered intraperitoneally every 24 hours for a period of two weeks. At the end of two weeks, the hanging wire test was performed again checking weight, glucose, and L-lactate before and after testing.

Treatment of ACAD9 deficient mice with XJB-5-131.

Twelve mice (7 wild type and 5 skeletal muscle specific ACAD9 deficient) were assessed with a hanging wire test as described above. XJB5-131 was added to DMSO at a final concentration of 1 μg/μL of DMSO and emulsified in 1 mL of PBS by several sonication. Injections of 2 mg/kg of body weight were administered intraperitoneally every 24 hours for a period of two weeks and animals were retested.

3.3 Specific Aim 2: Results

3.3.1 Treatment of wild type and skeletal muscle ACAD9 deficient mice with CLBP (RTP-03?).

Thirteen mice, six skeletal muscle tissue-specific ACAD9 deficient and seven wild type were assessed with a hanging wire test before and after two-weeks of treatment with CLBP (RTP-03?). As was seen in Specific Aim 1, the skeletal muscle ACAD9 deficient mice were unable to hold onto the wire for the full 3 minutes before falling 10 times prior to treatment, while all phenotypically normal animals successfully completed the test with few-to-no falls (Figure 29A). Mutant animals exhibited elevated L-lactate levels compared to wild type animals before and after the hanging wire test (Figure 30A), while glucose was unchanged in the mutant animals compared to wild type before and after the test (Figure 31A). Following treatment with the CLBP, there was no change in performance by mutant animals on the hanging wire test (Figure 29B), and lactometer and glucometer measurements from the blood showed that L-lactate and glucose levels were unaffected (Figures 30B and 31B).

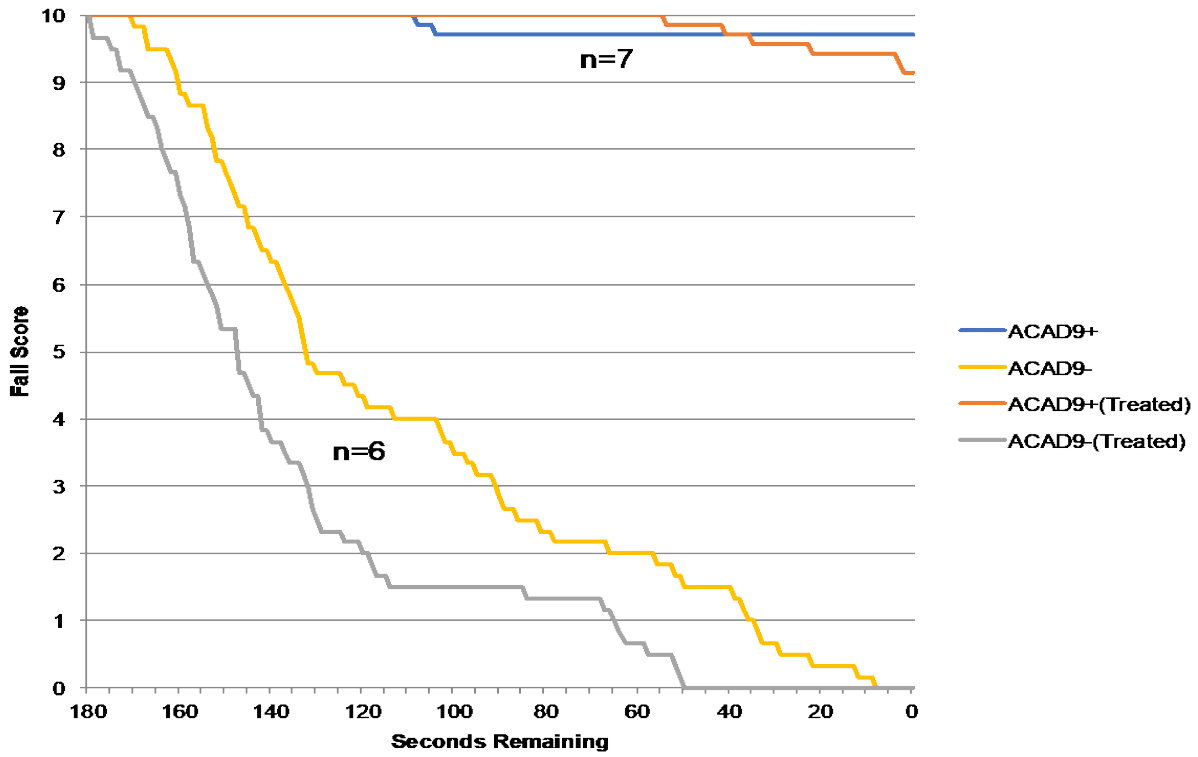

Figure 30 Hanging Wire Test of Skeletal Muscle-Specific ACAD9D (ACAD9-) and Wild Type (ACAD9+) Mice Before and After (Treated) 2 Weeks of Treatment with RTP-03

Mutant animals were unable to complete the hanging wire test, while most of the wild type animals did. The lines show the average fall score of all animals in all groups for each second. Average final fall scores indicate no significant difference between the treated and untreated animals. ACAD9+ mice were a collection of pooled normal mice from all experiments totaling seven mice. Six ACAD9- mice were used for the experiment. The p-value of time of final fall of ACAD9- mice before and after treatment was 0.35.

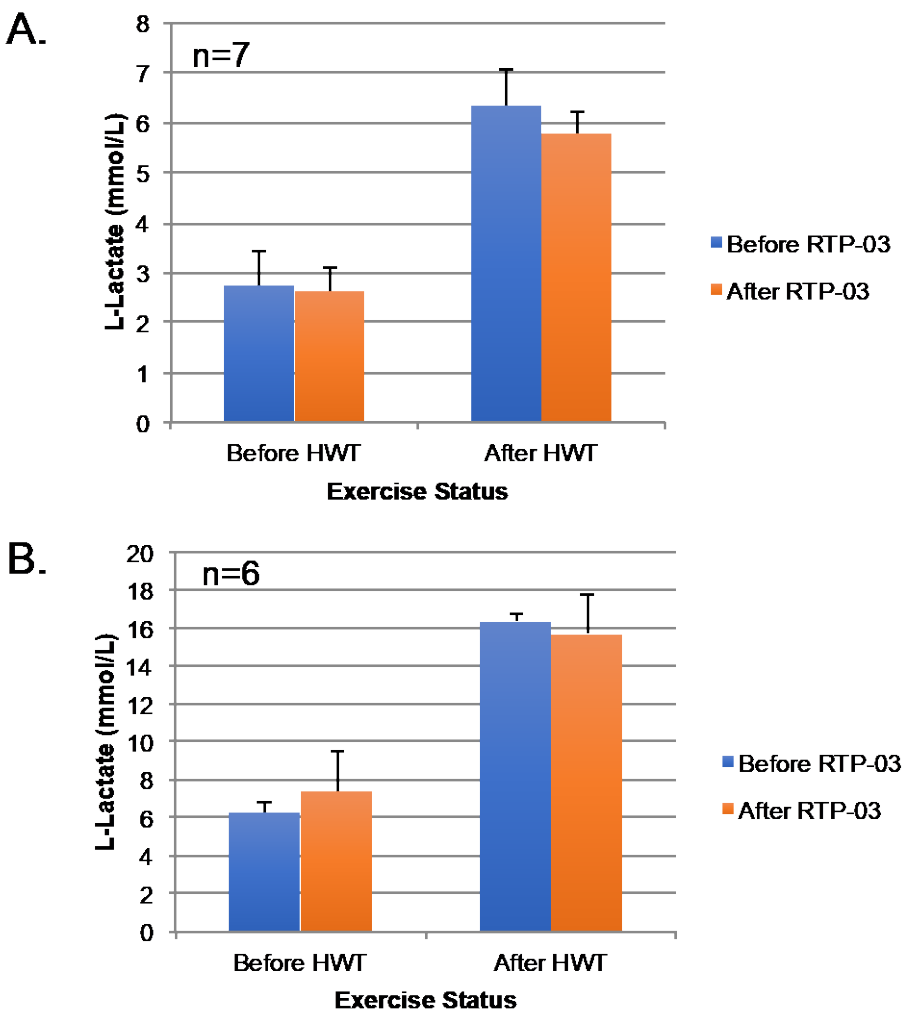

Figure 31 Blood L-Lactate in Wild Typre Mice (A) vs. Skeletal Muscle-Specific ACAD9 Deficient Mice (B) Before and After 2 Weeks of Treatment with RTP-03

Mean of L-lactate measurements from wild type (A) and mutant (B) animals. The error bars show 2 standard deviations from the mean. Mutant animals differ significantly from wild type before and after treatment, but showed no statistically significant change with treatment.

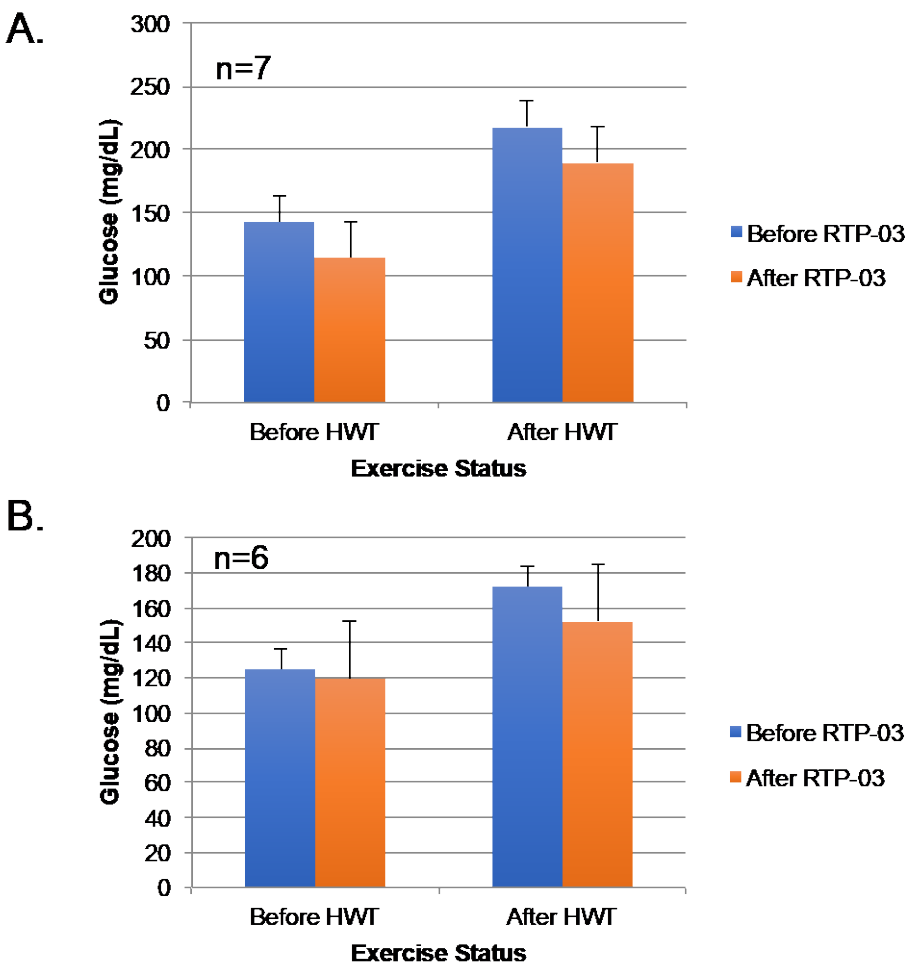

Figure 32 Blood Glucose Levels in Wild Type (A) and Skeletal Muscle-Specific ACAD9D Mice (B) Before and After 2 Weeks of Treatment with RTP-03

Glucose was measured before and after the hanging wire test. There was no observable difference in the change of glucose level before and after exercise after treatment with CBP.

3.3.2 Treatment of wild type and ACAD9 deficient mice with JP4-039.

I next tested the effect of JP4-039 treatment (5 mg/kg every 24 hours for 12 days) on wild type and muscle specific ACAD9 deficient animals with a hanging wire test as above. No difference in exercise performance as measured using the hanging wire test was observed as a result of the treatment, nor were blood glucose and L-lactate altered when measured using a glucometer and lactometer respectively (Figures 32-34).

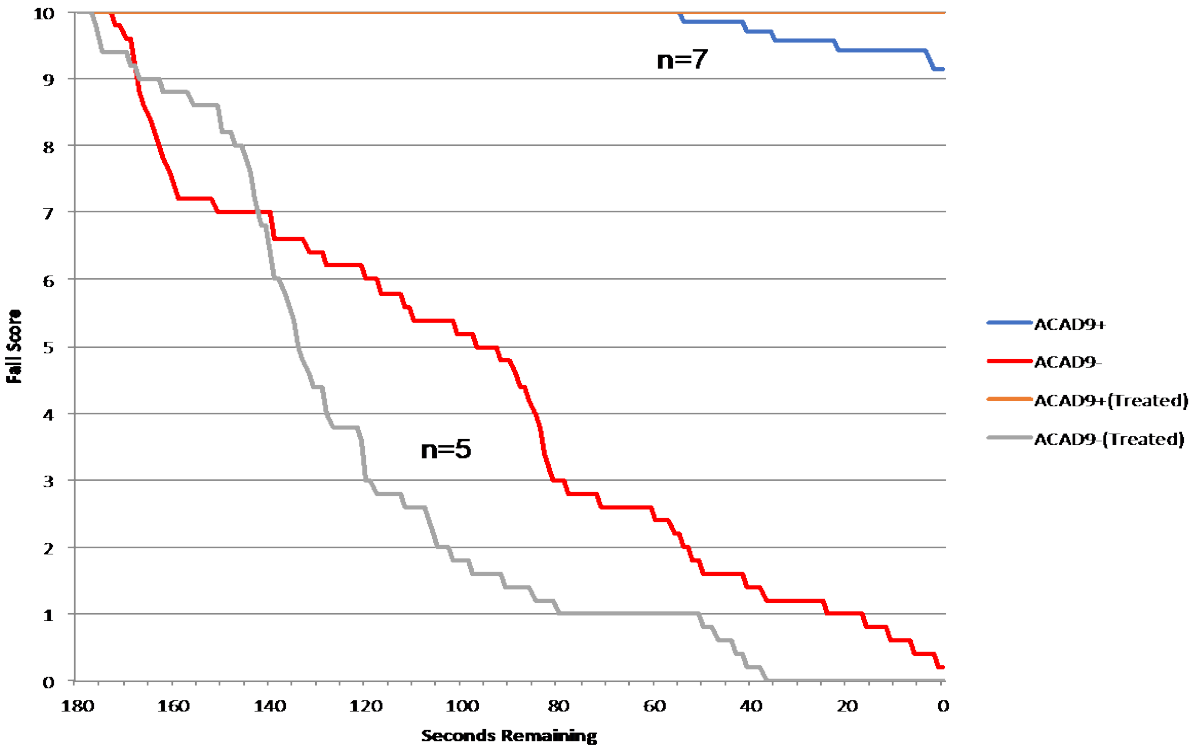

Figure 33 Hanging Wire Test of Skeletal Muscle-Specific ACAD9D (ACAD9-) and Wild Type (ACAD9+) Mice Before and After 2 Weeks of Treatment with JPR-039

Mutant animals were unable to complete the hanging wire test, while all of the wild type animals did. The lines show the cumulative fall score of all animals in both groups. Average final fall scores indicate no significant difference between the treated and untreated animals. ACAD9+ mice showed the same collection of pooled normal

mice from Figure 29 totaling seven mice. Five ACAD9- mice were used for the experiment. The p-value of time of final fall of ACAD9- mice before and after treatment was 0.15.

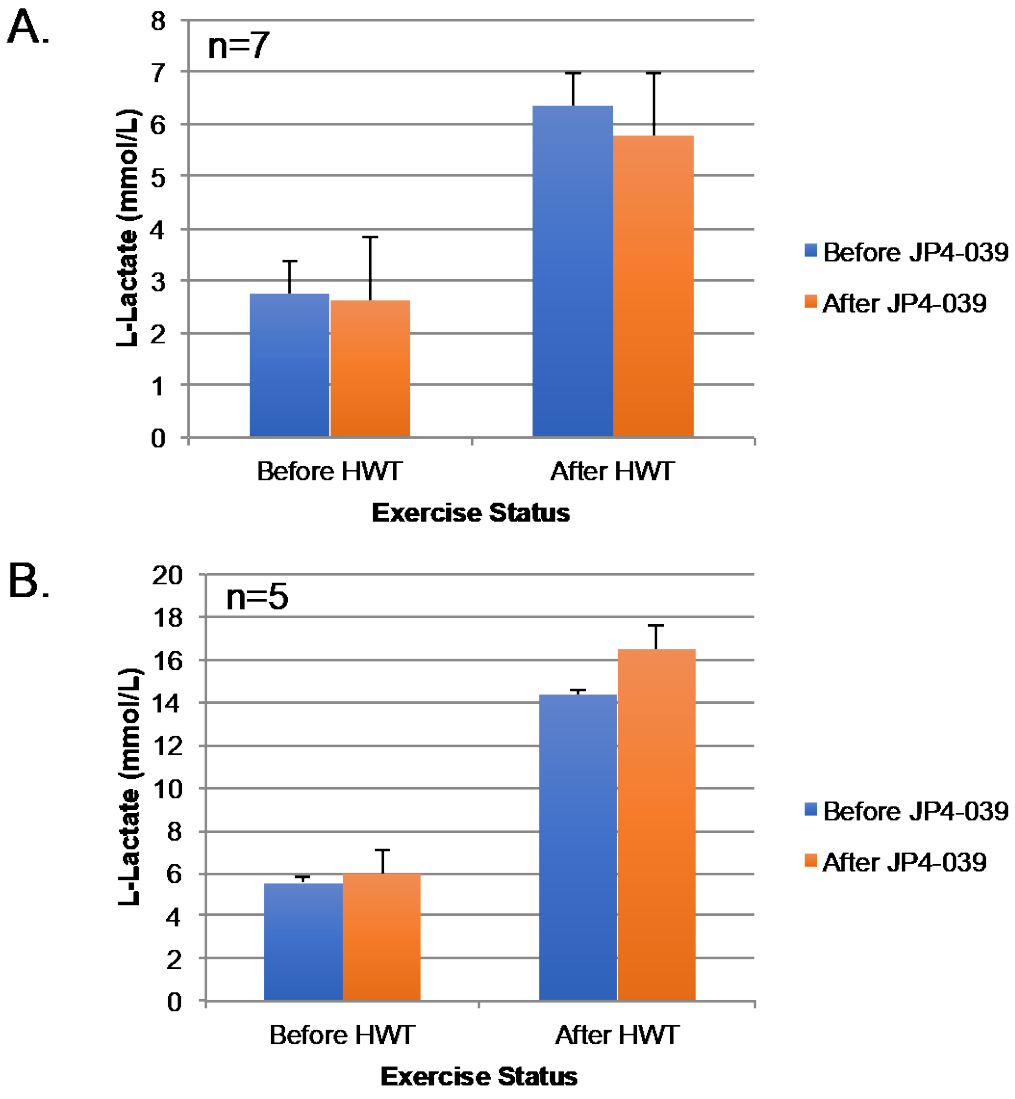

Figure 34 Blood L-Lactate in Wild Type Mice (A) and Skeletal Muscle-Specific ACAD9D Mice (B) Before and After 2 Weeks of Treatment with JP$-039

L-lactate was measured before and after the hanging wire test. While the increase in L-lactate after exercise is a measurable phenotype for the skeletal muscle-specific ACAD9 deficient mice, treatment with JP4 did not to improve the condition in any statistically significant manner.

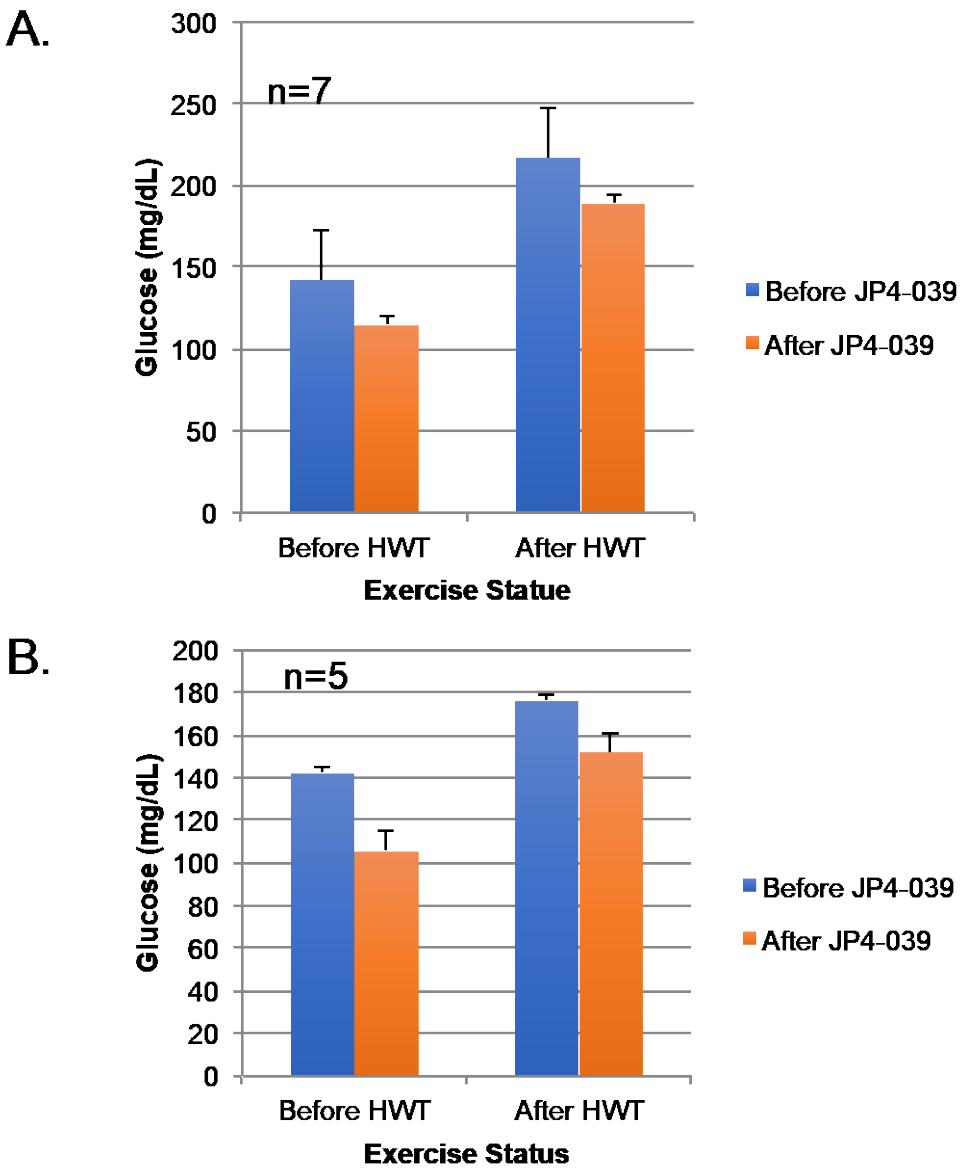

Figure 35 Blood Glucose Levels in Wild Type Mice (A) Skeletal Muscle-Specfic ACAD9D Mice (B) Before and After 2 Weeks of Treatment with JP4-039

Glucose was measured before and after the hanging wire test. As with CBP, JP4 did not appear to have any discernable effect on glucose level changes during exercise.

3.3.3 Treatment of skeletal muscle specific ACAD9 deficient and wild type mice with XJB-131-5.

XJB-131-5 is another synthetic antioxidant that reduces ROS subsequent damage to mitochondrial DNA.[26] Muscle specific ACAD9 deficient mice were treated for two weeks with this compound and compared to similarly treated wild type animals and tested as with JP4 and CBP treated animals. No significant differences were seen in hanging wire test performance, or in lactate or glucose levels before or after treatment (Figures 35-37)

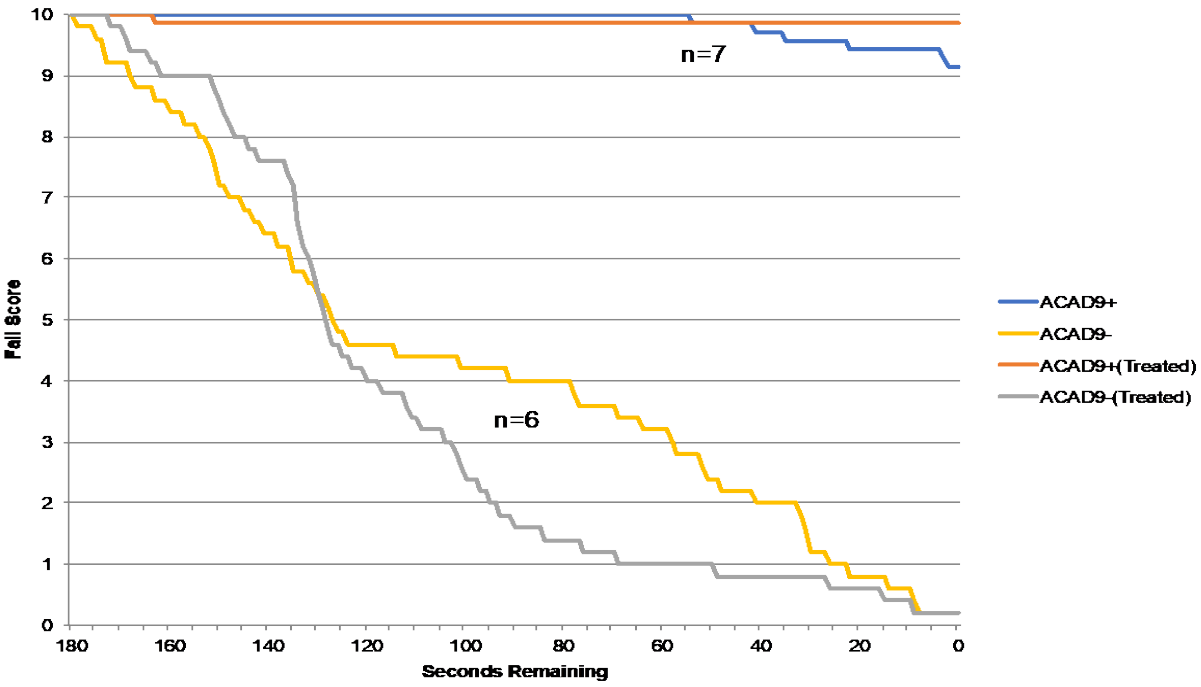

Figure 36 Hanging Wire Tests of Skeletal Muscle-Specific ACAD9D Mice Before and After (Treated) a 2 Week Treatment with XJB-5-131

XJB-131-5 did not improve performance of either ACAD9 deficient or wild type animals. Average final fall scores indicate no significant difference between the treated and untreated animals. ACAD9+ mice showed the same collection of pooled normal mice from Figure 29 totaling seven mice. Six ACAD9- mice were used for the experiment. The p-value of time of final fall of ACAD9- mice before and after treatment was 0.29.

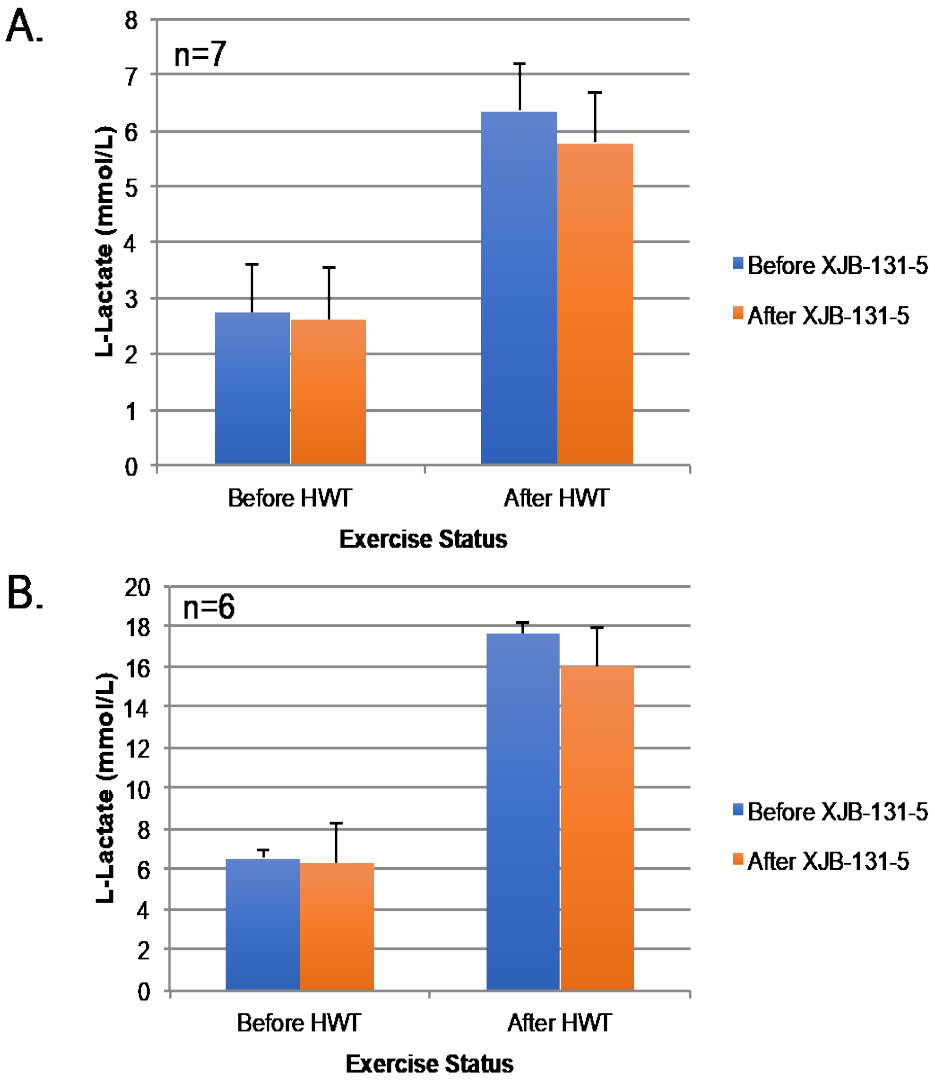

Figure 37 L-Lactate in Wild Type (A) and Skeletal Muscle-Specific ACAD9D Mice (B) Before and After a 2 Week Treatment with XJB-5-131

Measurements of L-lactate were made before and after the hanging wire test. No changes were seen with drug treatment.

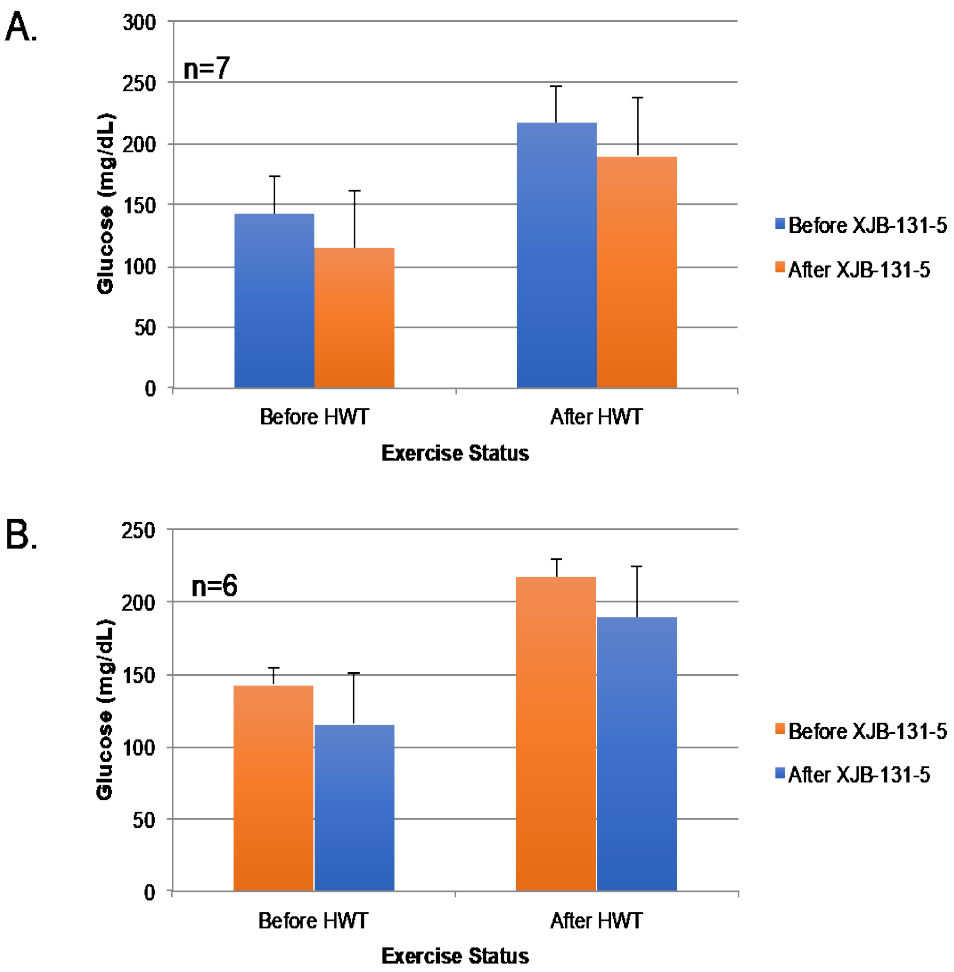

Figure 38 Glucose Levels in Wild Type (A) and Skeletal Muscle-Specific ACAD9D Mice (B) Before and After a 2 Week Treatment with XJB-5-131

Measurements of glucose were made before and after the hanging wire test and did not change with treatment.

3.4 Specific Aim 2: Discussion

None of the potential therapeutic compounds tested had a demonstrable effect on exercise capability as defined by completing the hanging wire test or blood L-lactate levels in mutant animals. A number of mechanisms of cellular pathophysiology are operative in the context of ETC deficiencies. First and foremost is a cellular deficit of energy. ETC functions at maximum efficiency through the macromolecular structures known as super complexes. A mutation in any ETC structural subunit will not only affect the function of the primary complex, but disruption of one complex has the potential to destabilize the entire super complex. Thus, in ACAD9 deficiency, any therapy that enhances complex I assembly is likely to increase super complex formation and increase energy production. Because my mice are knock out models, I do not expect to be able to affect this aspect of cellular pathophysiology. Fortunately, most mutations in patients with ACAD9 deficiency are point mutations and therefore may be responsive to therapy focused on stabilizing the super complexes. That being said, this is the first case of these compounds being tested on ACAD9D animals, and different trial parameters will need to be explored before a more concrete conclusion is established.

Cardiolipin has multiple chemically active bonds that can be oxidized by superoxides, leading to secondary structural changes in its structure, which in turn leads to destabilization of the inner mitochondrial membrane and ETC super complexes. RTP-03 is designed to restore the structure of oxidized cardiolipin and therefore improve inner mitochondrial membrane stability. While the compound had no effect in our mouse model, it was only tested at one concentration for relatively short duration. Subsequent experiments should test the effect of altering both variables on outcome. Additionally, it may be necessary to construct an ACAD9 deficient mouse model with a point mutation rather than a deletion to see an effect with the CLBP.

Loss of ETC complex or super complex integrity increases mitochondrial super oxide production that can lead to secondary damage of other mitochondrial proteins. Treatment of patients with cellular antioxidants have shown no efficacy in ETC deficiencies, presumably because of lack of effective delivery to mitochondria. JP4-039 and XJB-5-131 are more effectively targeted to mitochondria and should be of benefit in ETC deficiencies, preventing secondary damage. Only one concentration of each compound for one duration was tested in these experiments, leaving room for additional investigations.

Given that all three compounds have been shown in cellular systems to improve mitochondrial function in cellular systoms, lack of effect in ACAD9 deficient mice is somewhat surprising. While the complete loss of ETC function induced by ACAD9 deficiency may no be rescued by these treatmens, mutations in patients very rarely lead tot complete loss of function as they are likely lethal. Thus, generation of mice with ACAD9 point mutations with partial activity may provide a better system for testing therapeutic compounds.

Finally, none of these compounds were tested in the cardiac specific ACAD9 mice and it is possible that these animals will show effects under different treatment conditions, another avenue for future experiments.

4.0 Elucidating the Interaction of ECSIT in the Presence and Absence of ACAD9

The evolutionarily conserved signaling intermediate in the toll-pathway (ECSIT) protein was originally found to be associated with proteolytic activation of MAP3K1 in both the Il-1 toll-signaling pathway as well as the bone morphogenetic protein pathway (BMP)[31]. ECSIT's role in the BMP is directly related to embryonic formation of the mesoderm and is thus considered necessary for embryonic development[33]. It was later discovered to have a secondary function as a complex I assembly factor in tandem with NDUFAF1, a protein known to be associated with complex I assembly, when ECSIT was copurified along with a tandem affinity purification-tagged NDUFAF1 in HEK293 cells[34]. This study went on to show that ECSIT localizes to the mitochondria. Furthermore, study of ACAD9 deficient, HEK293 cells and fibroblast cell lines derived from ACAD9 patients have reduced ECSIT, as well as NDUFAF1[3,12]. This aim sought to better understand and characterize how these assembly factors interact with one another during the process of complex I formation.

4.1 Materials and Methods

Materials:

All items were purchased from Millipore Sigma, St. Louis, MO unless otherwise noted.

Immunofluorescence Staining of Paraffin-Embedded Mouse Heart and Skeletal Muscle Tissue

Slides contain paraffin-embedded tissues were prepared for immunofluorescence as in Specific Aim 1, reacted with primary antibodies to ACAD9 or ECIST, then reacted with fluorescently labeled secondary antibodies.

Western Blotting of Tissue Culture Cells

Control HEK293 cells, originally isolated as an embryonic kidney endothelial cells but more recently recognized to be of neuronal lineage, and cells with an ACAD9 gene deletion were grown to confluence, then lysed and processed for SDS-PAGE and western blotting as in Specific Aim 1.

Cloning and Culturing of DH5α *E. coli*

Mature human ACAD9 was inserted into the vector pET-21a+ vector (Novagen, Darmstadt, Germany) at the EcoRI restriction site. A single colony of *E. coli* grown on an agar plate was inoculated into 10 mL of liquid agarose media with 1% penicillin/streptomycin added and left to incubate in a standard shaker at 37 °C overnight. The saturated 10 mL of culture was then added to 500 mL of the same agarose media, included by the addition of IPTG and shaken

overnight at 37 °C. Finally, the 500 mL culture was moved to 12 L of 2X Yeast Extract/Tryptone (YT) liquid media and incubated with shaking at 37 °C overnight. The next morning, the cells were pelleted by low speed centrifugation and cell pellets were stored frozen until used.

Sf-21 Culture and Transfection with Baculovirus

Growth and baculovirus transfection of *Spodoptera frugiperda* (sf-21) insect cells were performed according to the Gibco Laboratories user guide (Thermofisher, Waltham, MA).

Fast Protein Liquid Chromatography

E coli pellets were thawed, resuspended in PBS buffer, pH 7.8, and lysed by several cycles of sonication on ice. Cellular debris was removed by centrifugation at 17,000 rpm (Sorvall RC5B Plus Refrigerated Centrifuge), and fractionated with a series chemical and chromatographic steps as follows. Ammonium sulfate fractionation (40-60%) was used to precipitate a large number of impurities such as lipids, glycolipids, and unwanted proteins. The presence of ACAD9 protein was monitored by SDS-PAGE and immunoblotting. The ammonium sulfate fraction containing ACAD9 was resuspended in PBS, pH 7.8 and fractionated on a DEAE Sepharose column (Amersham Biosciences. Waltham, MA), using a 0–500 mM NaCl gradient in 25 mM Tris (pH 8.0) for elution. Fractions with a yellow-green color characteristic of ACAD9 protein were tested for enzyme activity, and peak fractions were combined and loaded onto a hydroxyapatite column (BioRad. Hercules, CA). The column was eluted with a 0 – 0.5 mM potassium phosphate gradient at pH 7.0. Peak samples were pooled and concentrated by

ultrafiltration. All FPLC was conducted on a Pharmacia Fast protein Liquid Chromatography (FPLC) apparatus.

4.2 Specific Aim 3: Results

4.2.1 An Attempt to Purify ACAD9.

The Vockley lab has previously used expression in *E. coli* to generate large quantities of ACAD protein for subsequent purification. The sequence of mature human ACAD9 was inserted successfully into the prokaryotic expression vector (DH5α *E. coli*). The strain was seeded in 12 L cultures, the culture was induced with IPTG, the cell pellets were collected, and the presence of ACAD9 in the crude cellular extract was confirmed (Figure 38).

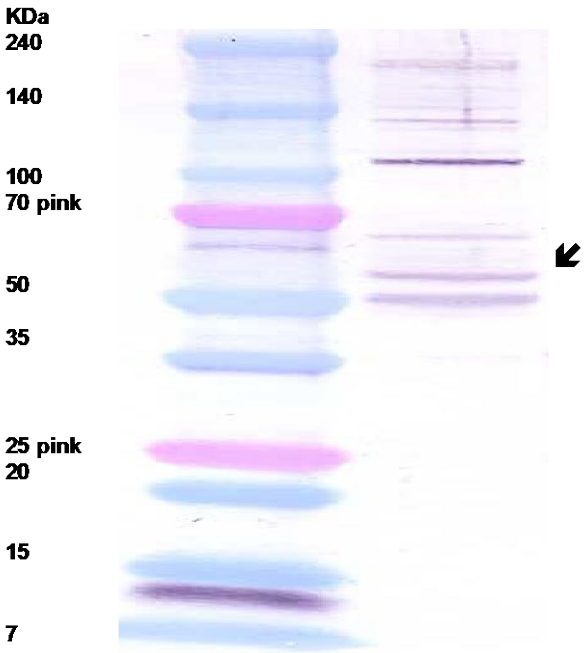

Figure 39 Confirmed Expression of ACAD9 in E. coli in Western Blot of Whole Cell Lysate (62 kDa)

Western blot confirmed the presence of ACAD9 in transformed *E. coli* after induction with IPTG. Whole cell lysate was obtained via centrifugation and sonication of pellets obtained from a 12L culture. The arrow indicates ACAD9.

Following ammonium sulfate fractionation, the sample was subjected to anion exchange chromatography using fast protein liquid chromatography and its presence was confirmed again (Figure 39). However, the subsequent ACAD9 protein proved to be unstable and could not be further purified by hydroxyapatite or cation exchange chromatography.

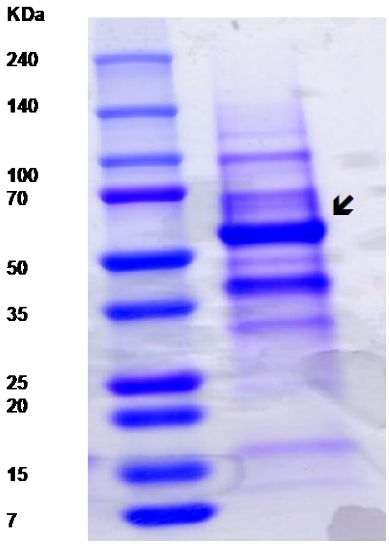

Figure 40 Coomassie Stain Confirming Presence of ACAD9 in E. coli Whole-Cell Lysate After DEAE Sepharose FPLC

After FPLC separation with a DEAE Sepharose column, ACAD9 (indicated by the arrow) visible in the column eluant (62KDa).

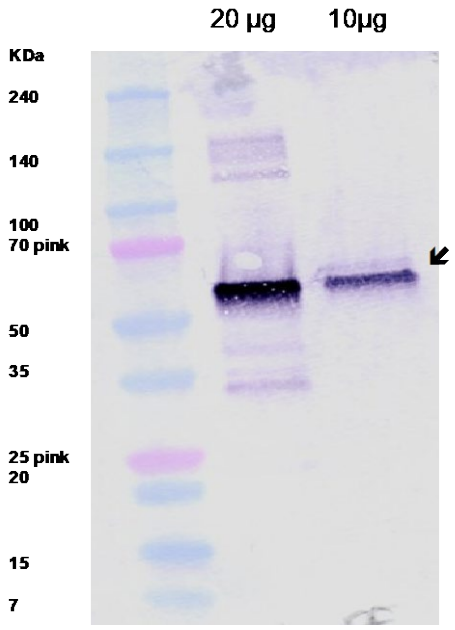

Figure 41 Western Blot for ACAD9 in Sf-21 Cells Using Whole Cell Lysate (62KDa)

Since purification of stable ACAD9 in *E. coli* proved to be problematic, an attempt was made to express the protein in insect cells using a baculovirus vector. Sf-21 insect cells were transfected with a copy of the precursor ACAD9 gene using a baculovirus vector. The insect cells are eukaryotic, thus can process the precursor ACAD9 protein to its mature intramitochondrial form. While transformed cells did produce ACAD9 (Figure 40), the protein yield was not sufficient for planned experiments and no purification was attempted.

4.2.2 Characterization of ACAD9 and ECIST Interactions in HEK 293 Cells

Cell lysates from HEK 293 and a previously generated ACAD9 deficient derivative were analyzed by SDS-PAGE and western blotting with antisera to ACAD9 and ECSIT. As previously reported, both ACAD9 and ECSIT were not detected in the ACAD9 deficient cell line (Figure 41). Immunohistochemistry imaging was also used to characterize the presense of both

proteins in the two cell lines. ACAD9 and ECSIT were found to colocalized to mitochondria in control cells and were both absent in the ACAD9 deficient cells (Figure 42).

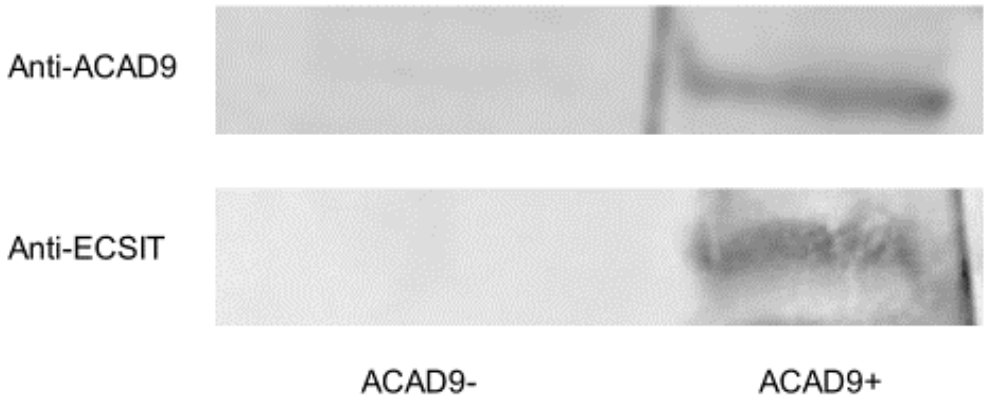

Figure 42 Western Blot Analysis of Control HEK293 Cell Lines and a Derivative with an ACAD9 Gene Deletion

Cell extracts were separated by SDS-PAGE, transferred to a membrane, then probed with ACAD9 and ECSIT antiserum. The top panel shows staining with the ACAD9 antiserum, while the bottom is stained with ECSIT antiserum. Both signals are missing from the left (ACAD deficient cells; left) and are present in the control cells (ACAD9+; right).

Next, tissue extracts from wild type and cardiac specific ACAD9 deficient tissues were analyzed by western blotting and immunohistochemistry. Western blotting showed that ACAD9 and ECSIT were both reduced compared to wild type tissue (Figure 43).

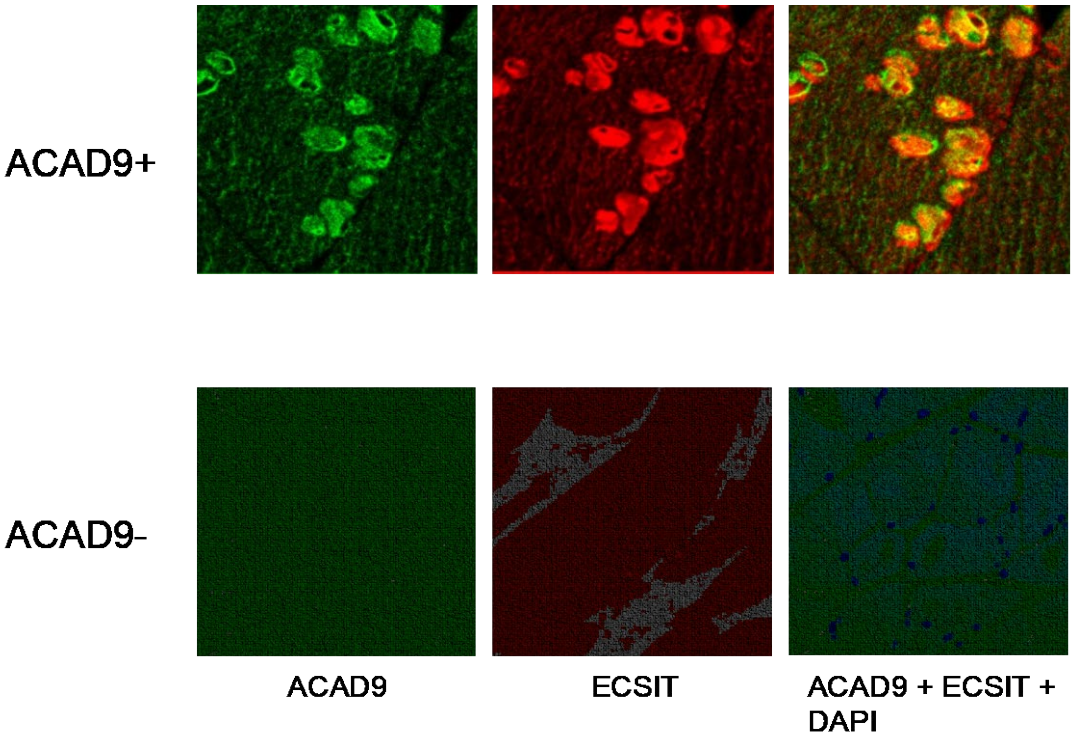

Figure 43 Immunohistochemistry Stains of Control and ACAD9D HEK293 Cell Lines

Cells were stained with ACAD9 antiserum (left panel) or ECSIT antiserum (center panel), then the images were merged (right panel). The yellow color indicates overlapping signals. The DAPI nuclear signal is blue. Control cell line images (top) were taken at 40x magnification while the ACAD9 deficient cell line images (bottom) were taken at 10X magnification to allow inclusion of more cells in the field of view.

Figure 44 Western Blot Analysis of ACAD9D Mouse Cardiac Tissue

Staining with ACAD9 and ECSIT antisera has yielded results which support the argument that when ACAD9 is not expressed as in the *Acad9* deficient mouse cardiac tissue, ECSIT protein expression is also reduced.

4.3 Specific Aim 3: Discussion

Initially, I attempted to express ACAD9 in *E. coli* in order to have a substantial supply for purification and X-ray crystallography studies. Unfortunately, ACAD9 was not sufficiently stable to purify under conditions that have been successful for other ACADs. I also attempted to express and purify ACAD9 from Sf-21 using a baculovirus system. While ACAD9 protein was identifiable in induced cells, the level was too low to allow ready purification and subsequent study. Further attempts at expression and purification of ACAD9 were abandoned to allow a focus on other more promising aspects of the project.

ECSIT and ACAD9 have been shown to be binding partners acting in the assembly of complex I. However, little else is known about this interaction. My findings confirm that ECSIT is unstable in ACAD9 deficient tissue culture cells and mouse tissues. Importantly, my ACAD9 deficient animals have the potential to be valuable tools to study complex I formation in general and ACAD9-ECSIT interactions specifically. In particular, an inducible ACAD9 deficient would allow timed studies of the dynamics of interaction of these two proteins and their relationship to the formation of normal super complexes (see Specific Aim 1 discussion). A better understanding of this process in turn has the potential to identify additional therapeutic targets at the molecular level to substitute for ACAD9 in complex I assembly and induce formation of ETC super complexes. Since some ACAD9 deficient patients have stable protein and no evidence of FAO deficiency, small molecules that would enhance the interaction of mutant ACAD9 with ECSIT would also improve complex I assembly, ETC super complex formation, and patient outcomes.

5.0 Overall Conclusions and Future Directions

In this thesis project, I have successfully created and characterized a set of mouse models for ACAD9 deficiency that share many characteristics of the human disorder. Tissue specific models also have provided insight into the cardiac and skeletal muscle dysfunction related to ACAD9 deficiency, and provide opportunities for pre-clinical testing of new therapies for this disorder. Initial therapeutic trials with the mitochondrial targeted antioxidants JP4-039 and XJB-5-131, and an elamipretide-like cardiolipin binding peptide failed to show benefit in skeletal muscle ACAD9 deficient but have provided insight into designing future studies of these compounds. Additionally, studies confirm the critical role of ACAD9 and ECSIT in complex I assembly and will provide novel tools for future experiments to better understand this process.

Because the Vockley lab's original whole body ACAD9 knock out mouse appeared to be embryonic lethal, I used Cre-lox technology to develop cardiac and skeletal muscle specific ACAD9 deficient animals that have allowed further study of these two organ systems critically affected in human patients. Development of these models substantiates the assumption that the original whole body knock out animal was embryonic lethal, although formal studies of mice immediately following establishment of a pregnancy will be necessary to unequivocally demonstrate the stage of loss of embryos. Regardless, these results are consistent with the conclusion that complete loss of ETC activity is incompatible with embryonic development.

My functional studies of cardiac specific ACAD9 deficient mice confirmed that they develop a severe hypertrophic cardiomyopathy that is lethal by three weeks of age. This cardiomyopathy is more severe than is seen in most ACAD9 deficient humans, likely explained by the variable severity of the (predominantly point) mutations present in human patients, many

of which lead to residual functional protein[57]. Nevertheless, the mouse model allowed confirmation of the complex I assembly function of ACAD9 *in vivo* in a setting that allowed survival through early postnatal development, and provides a model for future testing of potential therapeutic molecules. Indeed, given the relatively mild phenotype of the other two models developed in the project, the cardiac deficient ACAD9 mouse might ultimately prove to be the best model to study therapeutics. In this case, treatment form birth, or even prenatally, may allow improvement of early function and increase life span, a more easily scorable phenotype than is seen in muscle specific deficient mice.

The second model that I developed, a skeletal muscle tissue-specific ACAD9 deficient mouse, was viable, developed systemic lactic acidosis, and demonstrated exercise tolerance, consistent with disease symptoms in human patients. As in the cardiac deficient mice, skeletal muscle mice showed disruption of ETC super complexes; however, it is noteworthy that tissue morphology was more abnormal in the former than the latter animals. The reason for this finding is not clear, though it might have to do with the relative balance of energy metabolism, given that the heart is 70-80% reliant of fatty acid oxidation for energy generation. Because of their essentially normal life span, muscle specific ACAD9 deficient mice are an attractive model for studying therapy in an adult animal. While the phenotype (exercise intolerance) is less amenable to rapid studies, more subtle effects on ETC function and outcomes are more likely to be discernable than in the more severely affect cardiac animal. Additionally, while the exercise intolerance in the muscle ACAD9 deficient animals was easily discernable with the hanging wire test employed in this study, a wealth of other exercise measurements are available and can be considered as needed for future experiments.

My final model, a whole body inducible ACAD9 deficient mouse, proved to be a disappointment, showing no discernable biochemical, tissue, or functional phenotype. This finding was surprising given the embryonic lethal phenotype seen in constitutively ACAD9 deficient mice. However, identification of ACAD9 protein in tissue extracts of these animals six months after induction of the Cre allele with tamoxifen makes it clear that excision of the ACAD9 alleles was ineffective. Thus, to make this model useful, a more effective strategy for excision in the adult animals is necessary. The most logical approach to achieve this aim is to drive Cre with a stronger promotor, and indeed, such constructs have been reported to be more effective in obtaining efficient excision of a floxed gene in other studies.

Development of the skeletal muscle ACAD9 deficient mouse model allowed me to proceed to my second aim, testing novel therapeutic agents for treatment of this disorder. Previous studies in ACAD9 deficient cells in the Vockley lab had demonstrated that accumulation of mitochondrial superoxides is dramatic in ACAD9 deficient cells, and several potential therapeutic agents have shown promise in reversing this finding. All three of the agents used in this study (JP4-039, XJB-5-131, and RTP-03) showed promise in cell experiments. Based on the concentrations used in the cell experiments, I treated adult animals ages 2-6 months with each compound. Unfortunately, none of them had a significant positive impact on the exercise tolerance, or blood lactate levels of these mice after two weeks of treatment. There are several possible explanations for these findings. First, the compounds may truly not be effective. However, higher doses or longer treatment period may be necessary to see an effect. Follow up experiments in the Vockley Lab will explore these parameters. Finally, the complete tissue ACAD9 deficiency in these animals is representative of a minority of human patients, who have point mutations with potentially some residual function. It is possible that the secondary

mitochondrial dysfunction related to elevated superoxides is milder in this setting and would be more amenable to treatment. While generation of multiple mouse models to investigate this scenario is not feasible, cell studies with a series of point mutations in the ACAD9 gene could be created by CRISPR/cas9 technology, that could in turn be studied for functional effect of these and other therapeutic agents.

The moonlighting function of ACAD9 as an ETC complex I assembly factor and its interaction with ECSIT has only relatively recently been recognized and it is now clear that both ACAD9's enzymatic and chaperonin function are important in driving clinical phenotype. However, little is known about how these two critical proteins interact and how they are influence by other binding partners in the complex I assembly pathway. I originally proposed to study ACAD9/ECSIT binding *in vitro* by expressing and purifying wild type and mutant versions of each protein and characterizing their interactions directly. While ACAD9 has previously been expressed in an *E. coli* system in the Vockley lab, ACAD9 protein proved to be unstable, while baculovirus expression was too low to generate the quantities of protein necessary for my proposed experiments. Therefore, these experiments were ultimately abandoned as my mouse models reached fruition. Nevertheless, it is worth considering future options for studying ACAD9/ECSIT interactions. One possibility is to introduce specific mutations in one or both of these proteins into ACAD9 deleted cells, then characterize the effect on their binding and complex I assembly through functional assays of ETC activity. Alternatively, the binding of such proteins could be examined directly with such imaging techniques such as Förster resonance energy transfer FRET or stimulation emission depletion (STED) immunofluorescence that allow higher resolution assessment of protein interactions than was possible with the confocal techniques used in this project. Finally, proteomic studies of cross

linked mutant and wild type proteins could characterize the effects of ACAD9 and ECSIT mutations on interactions with each other, as well as other binding partners.

In conclusion, my thesis provides support for the role of ACAD9 as an ETC complex I assembly factor and insight to the clinical relevance of ACAD9 deficiency in humans. Whole body ACAD9 knock out animals did not survive embryogenesis, while cardiac and muscle specific ACAD9 deficient animals were viable. The former model proved to be clinically more severe, likely due to the reliance of the heart on FAO for energy. Initial treatment trials of the skeletal muscle deficient mouse with novel therapeutic agents failed to show an effect in the muscle deficient animals but identifies a path forward for additional treatment trials.

Bibliography

1. Ensenauer, R., He, M., Willard, J.-M., Goetzman, E. S., Corydon, T. J., Vandahl, B. B., Mohsen, A.-W., Isaya, G., Vockley, J. Human acyl-CoA dehydrogenase-9 plays a novel role in the mitochondrial beta-oxidation of unsaturated fatty acids. J. Biol. Chem. 280: 32309-32316, 2005.

2. Haack, T. B., Danhauser, K., Haberberger, B., Hoser, J., Strecker, V., Boehm, D., Uziel, G., Lamantea, E., Invernizzi, F., Poulton, J., Rolinski, B., Iuso, A., Biskup, S., Schmidt, T., Mewes, H.-W., Wittig, I., Meitinger, T., Zeviani, M., Prokisch, H. Exome sequencing identifies ACAD9 mutations as a cause of complex I deficiency. Nature Genet. 42: 1131-1134, 2010.

3. Chegary M, Brinke H te, Ruiter JPN, et al. Mitochondrial long chain fatty acid β-oxidation in man and mouse. *Biochimica et biophysica acta*. 2009;1791(8):806-815.

4. Grynberg, A, Demaison, L Fatty acid oxidation in the heart.. *J Cardiovasc Pharmacol*. (1996).

5. Berg JM, Tymoczko JL, Stryer L. Biochemistry. 5th edition. New York: W H Freeman; 2002. Section 30.2, Each Organ Has a Unique Metabolic Profile.

6. Moczulski D, Majak I, Mamczur D. An overview of beta-oxidation disorders. Postepy Hig Med Dosw (Online) 2009;63:266–77.

7. He, M., Rutledge, S. L., Kelly, D. R., Palmer, C. A., Murdoch, G., Majumder, N., Nicholls, R. D., Pei, Z., Watkins, P. A., Vockley, J. A new genetic disorder in mitochondrial fatty acid beta-oxidation: ACAD9 deficiency. Am. J. Hum. Genet. 81: 87-103, 2007.

8. Cooper GM. The Cell: A Molecular Approach. 2nd edition. Sunderland (MA): Sinauer Associates; 2000. The Mechanism of Oxidative Phosphorylation.

9. Spiekerkoetter, U., Lindner, M., Santer, R. et al. J Inherit Metab Dis (2009) 32: 498.

10. R.J. Janssen, L.G. Nijtmans, L.P. van den Heuvel, J.A. Smeitink Mitochondrial complex I: structure, function and pathology J. Inherit. Metab. Dis., 29 (2006), pp. 499–515.

11. V. Zickermann, S. Kerscher, K. Zwicker, M.A. Tocilescu, M. Radermacher, U. Brandt Architecture of complex I and its implications for electron transfer and proton pumping Biochim. Biophys. Acta, 1787 (2009), pp. 574–583.

12. Nouws J, Nijtmans L, Houten SM *et al*: Acyl-CoA dehydrogenase 9 is required for the biogenesis of oxidative phosphorylation complex I. Cell Metab 2010; 12: 283–294.

13. Collet, M., Assouline, Z., Bonnet, D., Rio, M., Iserin, F., Sidi, D., et al. (2016). High incidence and variable clinical outcome of cardiac hypertrophy due to ACAD9 mutations in childhood. *Eur. J. Hum. Genet.* 24, 1112–1116.

14. Haack, T. B., Haberberger, B., Frisch, E.-M., Wieland, T., Iuso, A., Gorza, M., Strecker, V., Graf, E., Mayr, J. A., Herberg, U., Hennermann, J. B., Klopstock, T., and 16 others. Molecular diagnosis in mitochondrial complex I deficiency using exome sequencing. J. Med. Genet. 49: 277-283, 2012.

15. Jia Zhang, Weiping Zhang, Dajin Zou, Guoyou Chen, Tao Wan, Minghui Zhang, Xuetao Cao, Cloning and functional characterization of ACAD-9, a novel member of human acyl-CoA dehydrogenase family, Biochemical and Biophysical Research Communications, Volume 297, Issue 4, 4 October 2002, Pages 1033-1042.

16. Swigonová Z, Mohsen AW, Vockley J. Acyl-CoA dehydrogenases: Dynamic history of protein family evolution. J Mol Evol. 2009 Aug;69(2):176-93.

17. Byers SL, Ficicioglu C. Infant with cardiomyopathy: When to suspect inborn errors of metabolism?. *World J Cardiol*. 2014 Nov 26. 6(11):1149-55.

18. He M, Burghardt TP, Vockley J. A novel approach to the characterization of substrate specificity in short/branched chain Acyl-CoA dehydrogenase. *J Biol Chem 2003*;*278*:*37974–*86.

19. Nouws J[1], Wibrand F, van den Brand M, Venselaar H, Duno M, Lund AM, Trautner S, Nijtmans L, Ostergard E. A Patient with Complex I Deficiency Caused by a Novel ACAD9 Mutation Not Responding to Riboflavin Treatment. JIMD Rep. 2014;12:37-45.

20. Louch WE, Sheehan KA, Wolska BM. Methods in Cardiomyocyte Isolation, Culture, and Gene Transfer. *Journal of molecular and cellular cardiology*. 2011;51(3):288-298. doi:10.1016/j.yjmcc.2011.06.012.

21. Van Putten, M. The use of hanging wire tests to monitor muscle strength and condition over time. Wellstone Muscular Dystrophy Center. DMD_M.2.1.004, 2011.

22. Epperly MW, Goff JP, Franicola D, Wang H, Wipf P, Li S, Greenberger JS: Esophageal radioprotection in thoracic-irradiated mice with transgenic lung tumors by swallowed JP4-039/.F15. In Vivo 28: 435-550, 2014

23. Voet, Donald, Judith Voet. Biochemistry, 3rd Edition. Wiley International Edition. 807-842. 2004.

24. Marcu CB, Beek AM, van Rossum AC. Clinical applications of cardiovascular magnetic resonance imaging. *CMAJ : Canadian Medical Association Journal*. 2006;175(8):911-917

25. Xun Z, Rivera-Sanchez S, Ayala-Penã S, et al. Targeting of XJB-5-131 to mitochondria suppresses oxidative DNA damage and motor decline in a mouse model of Huntington's disease. *Cell reports*. 2012;2(5):1137-1142.

26. Leipnitz G, Mohsen A-W, Karunanidhi A, et al. Evaluation of mitochondrial bioenergetics, dynamics, endoplasmic reticulum-mitochondria crosstalk, and reactive oxygen species in fibroblasts from patients with complex I deficiency. *Scientific Reports*. 2018;8:1165. doi:10.1038/s41598-018-19543-3

27. W. Epperly M, R. Sacher J, Krainz T, et al. Effectiveness of Analogs of the GS-Nitroxide, JP4-039, as Total Body Irradiation Mitigators. *In Vivo*. 2017;31(1):39-44. doi:10.21873/invivo.11022.

28. Xun Z, Rivera-Sanchez S, Ayala-Penã S, et al. Targeting of XJB-5-131 to mitochondria suppresses oxidative DNA damage and motor decline in a mouse model of Huntington's disease. *Cell reports*. 2012;2(5):1137-1142. doi:10.1016/j.celrep.2012.10.001.

29. Kloner RA, Shi J, Dai W. New therapies for reducing post-myocardial left ventricular remodeling. *Annals of Translational Medicine*. 2015;3(2):20. doi:10.3978/j.issn.2305-5839.2015.01.13.

30. Lenaz, G, Genova, ML. *Kinetics of integrated electron transfer in the mitochondrial respiratory chain: random collisions vs. solid state electron channeling.* American Journal of Physiology-Cell Physiology 2007 292:4, C1221-C1239.

31. Kopp E[1], Medzhitov R, Carothers J, Xiao C, Douglas I, Janeway CA, Ghosh S. ECSIT is an evolutionarily conserved intermediate in the Toll/IL-1 signal transduction pathway. Genes Dev. 1999 Aug 15;13(16):2059-71.

32. Wang Y, Mohsen A-W, Mihalik SJ, Goetzman ES, Vockley J. Evidence for Physical Association of Mitochondrial Fatty Acid Oxidation and Oxidative Phosphorylation Complexes. *The Journal of Biological Chemistry*. 2010;285(39):29834-29841. doi:10.1074/jbc.M110.139493.

33. Xiao C, Shim JH, Klüppel M, Zhang SS, Dong C, Flavell RA, Fu XY, Wrana JL, Hogan BL, Ghosh S (2003). Ecsit is required for Bmp signaling and mesoderm formation during mouse embryogenesis. **Genes Dev** *17*, 2933-2949.

34. Vogel RO, Janssen RJ, van den Brand MA, et al. Cytosolic signaling protein Ecsit also localizes to mitochondria where it interacts with chaperone NDUFAF1 and functions in complex I assembly. *Genes Dev*. 2007;21(5):615-24.

35. Carneiro FRG, Lepelley A, Seeley JJ, Hayden MS, Ghosh S. An Essential Role for ECSIT in Mitochondrial Complex I Assembly and Mitophagy in Macrophages. *Cell Rep*. 2018;22(10):2654-2666.

36. Y. Wang, A.-W. Mohsen, S.J. Mihalik, E.S. Goetzman, J. Vockley. Evidence for physical association of mitochondrial fatty acid oxidation and oxidative phosphorylation complexes. J. Biol. Chem., 285 (2010), pp. 29834-29841

37. Koopman WJ, Beyrath J, Fung CW, Koene S, Rodenburg RJ, Willems PH, Smeitink JA. Mitochondrial disorders in children: toward development of small-molecule treatment strategies. EMBO Mol Med 8: 311–327, 2016.

38. Repp BM, Mastantuono E, Alston CL, Schiff M, Haack TB, Rotig A, Ardissone A, Lombes A, Catarino CB, Diodato D, Schottmann G, Poulton J, Burlina A, Jonckheere A, Munnich A, Rolinski B, Ghezzi D, Rokicki D, Wellesley D, Martinelli D, Wenhong D, Lamantea E, Ostergaard E, Pronicka E, Pierre G, Smeets HJM, Wittig I, Scurr I, de Coo IFM, Moroni I, Smet J, Mayr JA, Dai L, de Meirleir L, Schuelke M, Zeviani M, Morscher RJ, McFarland R, Seneca S, Klopstock T, Meitinger T, Wieland T, Strom TM, Herberg U, Ahting U, Sperl W, Nassogne MC, Ling H, Fang F, Freisinger P, Van Coster R, Strecker V, Taylor RW, Haberle J, Vockley J, Prokisch H, Wortmann S. (2018). Clinical, biochemical and genetic spectrum of 70 patients with ACAD9 deficiency: is riboflavin supplementation effective? Orphanet J Rare Dis. **13:** 120. PMID 30025539.

39. Karaa A, Haas R, Goldstein A, Vockley J, Weaver WD, Cohen BH. Randomized dose-escalation trial of elamipretide in adults with primary mitochondrial myopathy. *Neurology*. 2018;90(14):e1212-e1221.

40. Mimaki, M. *et al*. Understanding mitochondrial complex I assembly in health and disease. Biochem. Biophys. Acta 1817, 851–862 (2012).

41. Oey, N. A., Ruiter, J. P. N., IJlst, L., Attie-Bitach, T., Vekemans, M., Wanders, R. J. A., Wijburg, F. A. Acyl-CoA dehydrogenase 9 (ACAD 9) is the long-chain acyl-CoA dehydrogenase in human embryonic and fetal brain. Biochem. Biophys. Res. Commun. 346: 33-37, 2006.

42. Zhang, J., Zhang, W., Zou, D., Chen, G., Wan, T., Zhang, M., Cao, X. Cloning and functional characterization of ACAD-9, a novel member of human acyl-CoA dehydrogenase family. Biochem. Biophys. Res. Commun. 297: 1033-1042, 2002.

43. Lodish H, Berk A, Zipursky SL, et al. Molecular Cell Biology. 4th edition. New York: W. H. Freeman; 2000. Section 3.5, Purifying, Detecting, and Characterizing Proteins.

44. Scopes RK. Overview of protein purification and characterization. Curr Protoc Protein Sci. 2001 May;Chapter 1:Unit 1.1.

45. Weiner DL. Inborn errors of metabolism. Aghababian RV, ed. *Emergency medicine: the core curriculum*. Philadelphia: Lippincott-Raven; 1999. 707.

46. Roomets E[1], Kivelä T, Tyni T. Carnitine palmitoyltransferase I and Acyl-CoA dehydrogenase 9 in retina: insights of retinopathy in mitochondrial trifunctional protein defects. Invest Ophthalmol Vis Sci. 2008 Apr;49(4):1660-4.

47. Ozlem Keskin, Nurcan Tuncbag, and Attila Gursoy Predicting Protein–Protein Interactions from the Molecular to the Proteome Level. Chemical Reviews 2016.

48. B. Xue, P.R. Romero, M. Noutsou, M.M. Maurice, S.G.D. Rüdiger, A.M. William Jr., *et al.* Stochastic machines as a colocalization mechanism for scaffold protein function. FEBS Lett, 587 (2013), pp. 1587–1591

49. Garone C[1], Donati MA, Sacchini M, Garcia-Diaz B, Bruno C, Calvo S, Mootha VK, Dimauro S. Mitochondrial encephalomyopathy due to a novel mutation in ACAD9. JAMA Neurol. 2013 Sep 1;70(9):1177-9.

50. Vaca Jacome AS, Rabilloud T, Schaeffer-Reiss C, Rompais M, Ayoub D, Lane L, Bairoch A, Van Dorsselaer A, Carapito C. N-terminome analysis of the human mitochondrial proteome. Proteomics. 2015 Jul;15(14):2519-24

51. Agrawal P[1], Yu K, Salomon AR, Sedivy JM. Proteomic profiling of Myc-associated proteins. Cell Cycle. 2010 Dec 15;9(24):4908-21. Epub 2010 Dec 15

52. Calvo SE, Compton AG, Hershman SG, Lim SC, Lieber DS, Tucker EJ, Laskowski A, Garone C, Liu S, Jaffe DB, Christodoulou J, Fletcher JM, Bruno DL, Goldblatt J, Dimauro S, Thorburn DR, Mootha VK. Molecular diagnosis of infantile mitochondrial disease with targeted next-generation sequencing. Sci Transl Med. 2012 Jan 25

53. Havugimana PC, Hart GT, Nepusz T, Yang H, Turinsky AL, Li Z, Wang PI, Boutz DR, Fong V, Phanse S, Babu M, Craig SA, Hu P, Wan C, Vlasblom J, Dar VU, Bezginov A, Clark GW, Wu GC, Wodak SJ, Tillier ER, Paccanaro A, Marcotte EM, Emili A. A census of human soluble protein complexes. Cell. 2012 Aug 31;150(5):1068-81.

54. Gerards M, van den Bosch BJ, Danhauser K *et al*: Riboflavin-responsive oxidative phosphorylation complex I deficiency caused by defective ACAD9: new function for an old gene. Brain 2011; 134: 210–219.

55. Nouws J[1], Te Brinke H, Nijtmans LG, Houten SM. ACAD9, a complex I assembly factor with a moonlighting function in fatty acid oxidation deficiencies. Hum Mol Genet. 2014 Mar 1;23(5):1311-9.

56. Seminotti B, Leipnitz G, Karunanidhi A, Kochersperger C, Roginskaya VY, Basu S, Wang Y, Wipf P, Van Houten B, Mohsen AW, Vockley J. (2018). Mitochondrial energetics is impaired in very long-chain acyl-CoA dehydrogenase deficiency and can be rescued by treatment with mitochondria-targeted electron scavengers. *Human Molecular Genetics.*

57. Repp BM, Mastantuono E, Alston CL, Schiff M, Haack TB, Rotig A, Ardissone A, Lombes A, Catarino CB, Diodato D, Schottmann G, Poulton J, Burlina A, Jonckheere A, Munnich A, Rolinski B, Ghezzi D, Rokicki D, Wellesley D, Martinelli D, Wenhong D, Lamantea E, Ostergaard E, Pronicka E, Pierre G, Smeets HJM, Wittig I, Scurr I, de Coo IFM, Moroni I, Smet J, Mayr JA, Dai L, de Meirleir L, Schuelke M, Zeviani M, Morscher RJ, McFarland R, Seneca S, Klopstock T, Meitinger T, Wieland T, Strom TM, Herberg U, Ahting U, Sperl W, Nassogne MC, Ling H, Fang F, Freisinger P, Van Coster R, Strecker

V, Taylor RW, Haberle J, Vockley J, Prokisch H, Wortmann S. (2018). Clinical, biochemical and genetic spectrum of 70 patients with ACAD9 deficiency: is riboflavin supplementation effective? Orphanet J Rare Dis. 13: 120. PMID 30025539.

58 .Heide H1, Bleier L, Steger M, Ackermann J, Dröse S, Schwamb B, Zörnig M, Reichert AS, Koch I, Wittig I, Brandt U. Complexome profiling identifies TMEM126B as a component of the mitochondrial complex I assembly complex. Cell Metab. 2012 Oct 3;16(4):538-49

59. Schiff M, Haberberger B, Xia C, et al. Complex I assembly function and fatty acid oxidation enzyme activity of ACAD9 both contribute to disease severity in ACAD9 deficiency. *Human Molecular Genetics*. 2015;24(11):3238-3247.